Journal of Sedimentary Research

Journal of Sedimentary Research, 2010, v. 80, 955–974
Research Article
DOI: 10.2110/jsr.2010.086

CORRELATION OF APTIAN–ALBIAN CARBON ISOTOPE EXCURSIONS IN CONTINENTAL STRATA OF THE CRETACEOUS FORELAND BASIN, EASTERN UTAH, U.S.A.

GREG A. LUDVIGSON,[1] R.M. JOECKEL,[2] LUIS A. GONZÁLEZ,[3] ERIK L. GULBRANSON,[4] E. TROY RASBURY,[5] GARY J. HUNT,[6] JAMES I. KIRKLAND,[7] AND SCOTT MADSEN[7]

[1]*Kansas Geological Survey, University of Kansas, Lawrence, Kansas 66047, U.S.A.*
[2]*Conservation and Survey Division, School of Natural Resources and Department of Earth and Atmospheric Sciences, University of Nebraska, Lincoln, Nebraska 68583, U.S.A.*
[3]*Department of Geology, University of Kansas, Lawrence, Kansas 66045, U.S.A.*
[4]*Department of Geology, University of California-Davis, Davis, California 95616, U.S.A.*
[5]*Department of Geosciences, Stony Brook University, Stony Brook, New York 11794, U.S.A.*
[6]*Department of Geological Sciences, New Mexico State University, Las Cruces, New Mexico 88003, U.S.A.*
[7]*Utah Geological Survey, Salt Lake City, Utah 84114, U.S.A.*
e-mail: gludvigson@kgs.ku.edu

ABSTRACT: **Nodular carbonates ("calcretes") in continental foreland-basin strata of the Early Cretaceous Cedar Mountain Formation (CMF) in eastern Utah yield $\delta^{13}C$ and $\delta^{18}O$ records of changes in the exogenic carbon cycle related to oceanic anoxic events (OAEs), and terrestrial paleoclimate. Chemostratigraphic profiles of both forebulge and foredeep sections show two prominent positive $\delta^{13}C$ excursions, each with a peak value of −3‰ VPDB, and having background $\delta^{13}C$ values of about −6‰ VPDB. These excursions correlate with the global early Aptian (Ap7) and late Aptian–early Albian (Ap12–Al1) carbon isotope excursions. Aptian–Albian positive $\delta^{13}C$ excursions in the CMF also correspond to 3–4 per mil increases in carbonate $\delta^{18}O$. These phenomena record local aridification events. The chemostratigraphic profile on the thinner forebulge section of the CMF is calibrated, for the first time, by a radiogenic U-Pb date of 119.4 ± 2.6 Ma on a carbonate bed, and by detrital zircon U-Pb dates on two bounding sandstone units (maximum depositional ages of 146 Ma and 112 Ma). Petrographic observations and diagenetic analyses of micritic to microsparitic carbonates from nodules indicate palustrine origins and demonstrate that they crystallized in shallow early meteoric phreatic environments. Meteoric calcite lines derived from CMF carbonates have $\delta^{18}O$ values ranging between −8.1 to −7.5‰ VPDB, supporting an estimate of zonal mean groundwater $\delta^{18}O$ of −6‰ VSMOW for an Aptian–Albian paleolatitude of 34° N. Furthermore, our two chemostratigraphic profiles exhibit a generally proportionate thinning of correlative strata from the foredeep on to the forebulge, suggesting that there were consistently lower rates of accumulation on the forebulge during the Aptian–Albian. Identification of the global Aptian–Albian $\delta^{13}C$ excursions in purely continental strata, as demonstrated in this paper, opens a new avenue of research by identifying specific stratigraphic intervals that record the terrestrial paleoclimatic impacts of perturbations of the global carbon cycle.**

INTRODUCTION

The Problem of Terrestrial Correlation of Carbon Isotope Excursions

Carbon isotope excursions (CIEs) associated with the mid-Cretaceous Oceanic Anoxic Events (OAEs) were major episodes of global change (Dumitrescu et al. 2006; Wagner et al. 2008; Ando et al. 2008; Hofmann et al. 2008). Previous studies (Hasegawa 1997; Gröcke et al; 1999; Jahren et al. 2001; Gröcke 2002; Ando et al. 2002; Heimhofer et al. 2003; Jacobs et al. 2005; Gröcke et al. 2006) indirectly correlated continental and marine records of CIEs by analyzing terrestrial plant carbon in marine strata. These studies are ultimately limited in impact because they cannot assess the terrestrial paleoclimatic impacts of the CIEs. In contrast, we present carbon isotope chemostratigraphic studies of two Aptian–Albian stratigraphic sections in the fully terrestrial Cedar Mountain Formation (Fig. 1), and integrate chemostratigraphic profiles derived from carbonate components with radiometric U-Pb dates to correlate them with global carbon isotope chemostratigraphy. Only in this manner will it eventually be possible to accurately correlate CIEs from marine to terrestrial strata, and assess the direct impacts of the CIEs on terrestrial paleoclimates.

A Solution in Terrestrial Carbonate Chemostratigraphy

The Lower Cretaceous Cedar Mountain Formation (CMF) in eastern Utah (Kirkland et al. 1997) provides an ideal setting in which to address the problem of terrestrial correlation of CIEs. The CMF contains abundant nodular carbonates of palustrine origin ("calcretes") with carbonate cements filling both synsedimentary voids and post-lithification tectonic veins (Kirkland et al. 1997; Ludvigson et al. 2003). Nodular palustrine carbonates (e.g., Platt and Wright 1992), are known to capture highly resolved records of global carbon isotope excursions in continental strata (Cojan et al. 2000; Bains et al. 2003). We produced stable-isotope chemostratigraphic profiles by repetitively microsampling micritic and microsparitic components in the CMF carbonate nodules, and then we

 1527-1404/10/080-955/$03.00

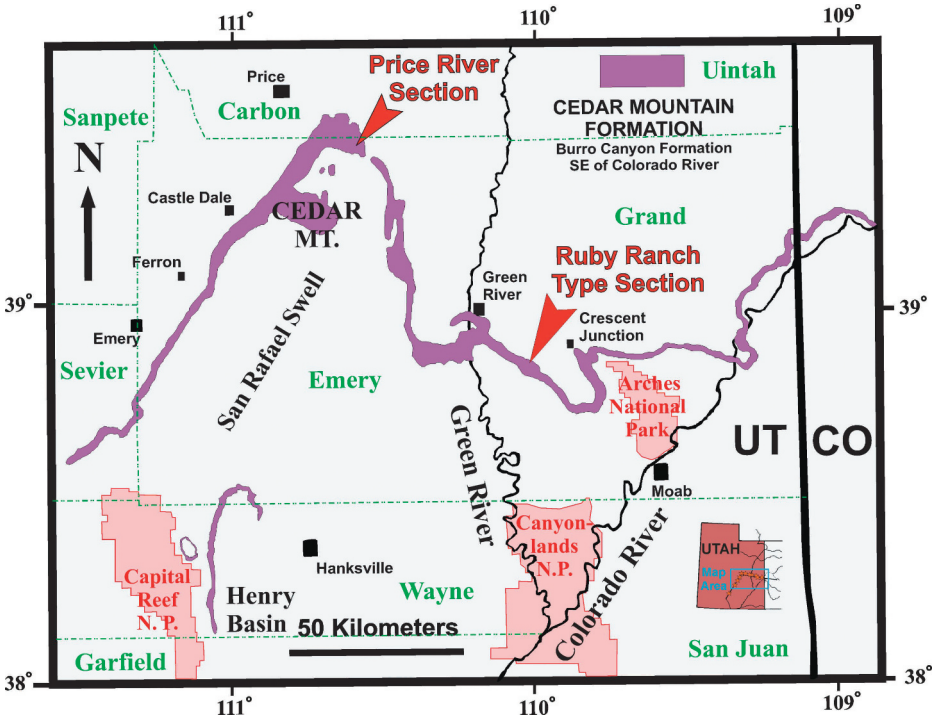

FIG. 1.—Location map for the Price River and Ruby Ranch Road (type section of the Ruby Ranch Member) sections, in relation to the outcrop area of the Early Cretaceous Cedar Mountain Formation (after Currie 2002; Sprinkel et al. 1999; Kirkland and Madsen 2007).

assessed the resultant diagenetic trends relative to data derived from microsampling the void-filling cements. Through this comprehensive analysis, we distinguish both early and late diagenetic products and processes. We can also relate chemostratigraphic profiles from the CMF to the contemporaneous global $\delta^{13}C$ chronology.

GEOLOGIC SETTING OF THE CEDAR MOUNTAIN FORMATION

In the study area (Fig. 1), the Cedar Mountain Formation comprises: (1) sandy to gravelly fluvial channel fills, bar deposits, and associated coarser-grained deposits; (2) overbank mudrocks, which account for most of the volume of the unit, and (3) nodular palustrine carbonates, commonly referred to by the nonspecific term "calcretes" (Currie 1998). Modifying the stratigraphic scheme of Sprinkel et al. (1999), paleontologists (Kirkland et al. 1997; Kirkland and Madsen 2007) have subdivided the CMF into the Yellow Cat, Poison Strip Sandstone, Ruby Ranch, and Mussentuchit members (Fig. 2). Biostratigraphic and radiometric data attributing an Early Cretaceous—possibly Barremian through earliest Cenomanian age—to most of the Cedar Mountain Formation were attained only after 1980 (Sprinkel et al. 1999), and continue to accumulate to the present day (e.g., Cifelli et al. 1997; Cifelli et al. 1999; Dickinson and Gehrels 2008; Greenhalgh et al. 2006; Garrison et al. 2007). Important finds of dinosaur fossils in the Cedar Mountain Formation make the reevaluation of chronostratigraphy a critically important task (Kirkland and Madsen 2007).

Yellow Cat Member.—The Yellow Cat Member is dominated by grayish to greenish massive mudstones containing nodules of micritic to microsparitic carbonate, which reach diameters of several centimeters (Kirkland and Madsen 2007). Greenhalgh et al. (2006) derived a U-Pb maximum depositional age of 126 ± 2.5 Ma for the Yellow Cat Member from detrital zircons, and a later report of a 124 +2/−2.8 Ma date at the base of the Yellow Cat Member at Dinosaur National Monument was made by Britt et al. (2007). These dates are consistent with vertebrate biostratigraphic data (Kirkland and Madsen 2007). The assemblage of dinosaurs from the Yellow Cat Member, in comparison with Early Cretaceous European dinosaur faunas, as well as occurrences of zonally significant palynomorphs and charophytes, are compatible with an age assignment of ~ 125–120 Ma (Kirkland et al. 1993; Cifelli et al. 1997; Galton and Jensen 1979; Britt et al. 1997; Britt and Stadtman 1997; Kirkland et al. 1997; Kirkland et al. 1998; Kirkland et al. 1999; Kirkland 2005; Tidwell et al. 1999; Eberth et al. 2006). Hybodont sharks, lungfish, semionotid fishes, turtles, crocodilians, a neochoristodere, and a large sphenodontian (*Toxolophosaurus*?) have also been found in the Yellow Cat Member (Kirkland and Madsen 2007).

Our observations of the Yellow Cat Member come from many partially covered slopes and a few very well-exposed vertical exposure faces. Reddish, massive, blocky-weathering mudstones with secondary carbonate nodules—analogous to carbonate nodules found in modern Vertisols—are common. Drab (grayish to greenish), massive, blocky-weathering mudstones appear to be less common. In the best exposures of reddish, massive mudstones with minor drab horizons near the top of the Yellow Cat Member, vertic soil features such as cyclic synformal sets of large slickensides, intersecting at prominent peaks, fine to coarse wedge-shaped soil aggregates, and large filled cracks are common in massive mudstones. Lenticular to sheet-like fine to medium sandstones are interspersed between mudrock intervals in this part of the unit, and some fine sandstones lack primary bedding, appear to be bioturbated or otherwise mixed by physical processes, are thoroughly mottled, and also contain vertical trains of secondary carbonate nodules.

Poison Strip Sandstone.—The Poison Strip Sandstone is a complex of ledge-forming medium to coarse sandstones of dominantly of fluvial origin (Stikes 2006). Dinosaur fossils suggest an affinity with the fauna from the Yellow Cat Member (Bodily 1969; Carpenter et al. 1999).

Ruby Ranch Member.—The Ruby Ranch Member, like the Yellow Cat Member, consists largely of massive mudstones with large nodules of secondary carbonate. A comparison of the Ruby Ranch Member dinosaur assemblage with similar dinosaur faunas from North America indicates an age assignment of ~ 115–105 Ma (Kirkland et al. 1998).

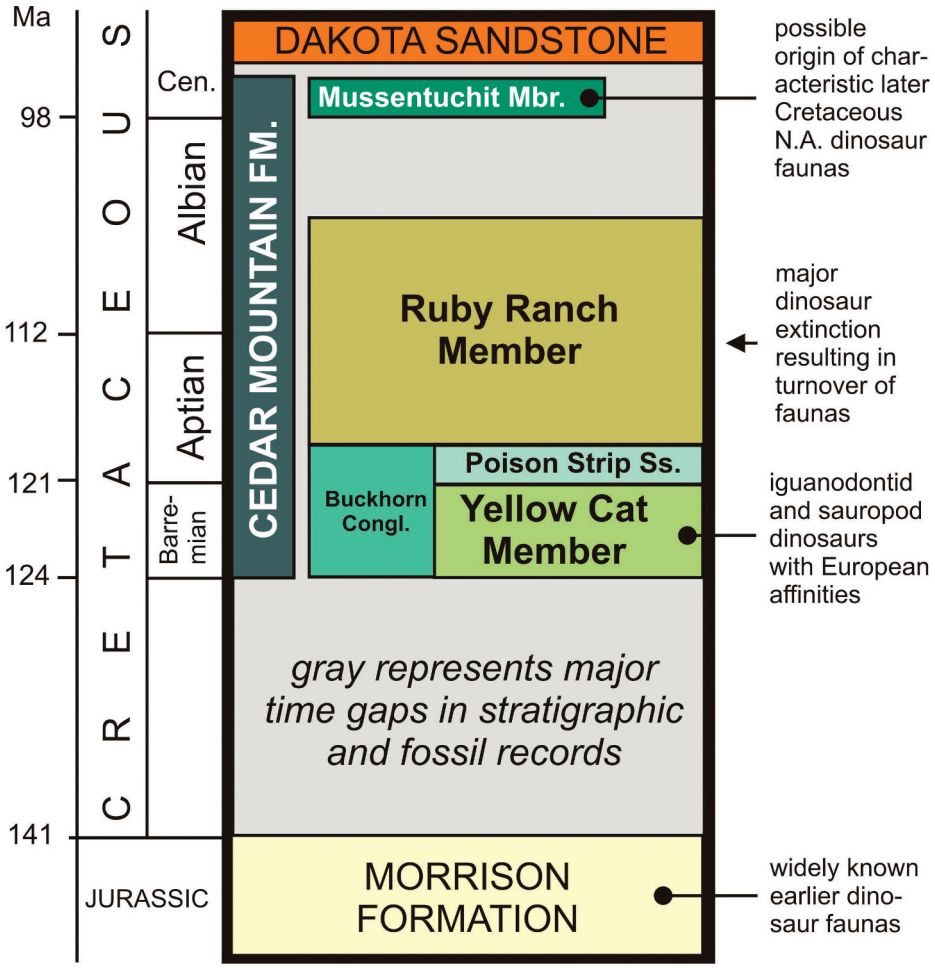

FIG. 2.—Stratigraphy of the Early Cretaceous Cedar Mountain Formation (after Kirkland et al. 1997).

Endemic North American dinosaur taxa in the Ruby Ranch Member record the isolation of North America from Europe.

Our observations of the Ruby Ranch Member indicate that reddish colors are more prominent than drab (grayish to greenish) ones, although drab colors dominate locally. Common, irregularly shaped nodules of dense micritic carbonate in the Ruby Ranch Member attain dimensions of several centimeters to a few tens of centimeters. Continuous layers of authigenic carbonate or horizons of dense or intergrown spheroidal to cylindroidal carbonate nodules (“calcretes”), are prominent at multiple levels. These “calcretes” contain features diagnostic of palustrine deposition (cf. Shapiro et al. 2009; Garrison et al. 2007). Nonetheless, we also interpret some vadose features in these carbonates.

Mussentuchit Member.—The Mussentuchit Member is dominated by “popcorn”-weathering smectitic mudstones and shales and also contains nodules of micritic–microsparitic carbonate. Volcanic ash in the Mussentuchit Member has yielded a radiometric age of 98.37 ± 0.07 Ma (Cifelli et al. 1997; Cifelli et al. 1999), which was subsequently amended by several ash dates ranging between 98.5 to 96.7 Ma (Garrison et al. 2007). A palynomorph assemblage from the Mussentuchit Member suggests an early Cenomanian age in comparison with ammonite correlations in Europe (Tschudy et al. 1984; Cobban and Kennedy 1989; Nichols and Sweet 1993). The occurrence of Asiatic dinosaurs in the Mussentuchit Member, such as tyrannosaurids and the hadrosaur *Eolambia*, as well as the occurrence of the marsupial mammal *Kokopellia juddi*, have been cited as direct evidence for the reopening of a land connection between Asia and North America (Cifelli and de Muizon 1997), and thereby provide additional chronological context. Furthermore, the Mussentuchit Member dinosaur fauna can be considered the earliest known occurrence of the distinctively Late Cretaceous North American dinosaur fauna (Cifelli et al. 1997).

Paleogeography and Tectonism.—The entire Lower Cretaceous succession in Utah thins markedly eastward from the front of the Sevier Thrust Belt (Currie 2002). Flexural subsidence during the Early Cretaceous created more accommodation space west of the present San Rafael Swell, whereas the development of a flexural forebulge led to the overall thinning of age-equivalent strata in eastern Utah and western Colorado (Currie 2002). Our Price River (PR) section was located at the very eastern edge of the foredeep in front of the Sevier Thrust Belt (Fig. 3), whereas the Ruby Ranch Road (RRR) section was located over the forebulge; therefore, the greater thickness of equivalent stratigraphic section at Price River (versus Ruby Ranch Road) reflects the generation of more accommodation space there. Paleocurrent data indicate northward to eastward streamflow emerging from the thrust belt and crossing the foreland basin (Currie 2002). Actively uplifting mountains immediately to the west doubtless exerted an orographic effect on the foreland basin (cf. Elliot et al. 2007).

METHODS OF INVESTIGATION

Stable-Isotope Studies

In the laboratory, rock samples were cleaned, dried, and coated with epoxide resins, and then they were then cut into slabs about 1 cm thick,

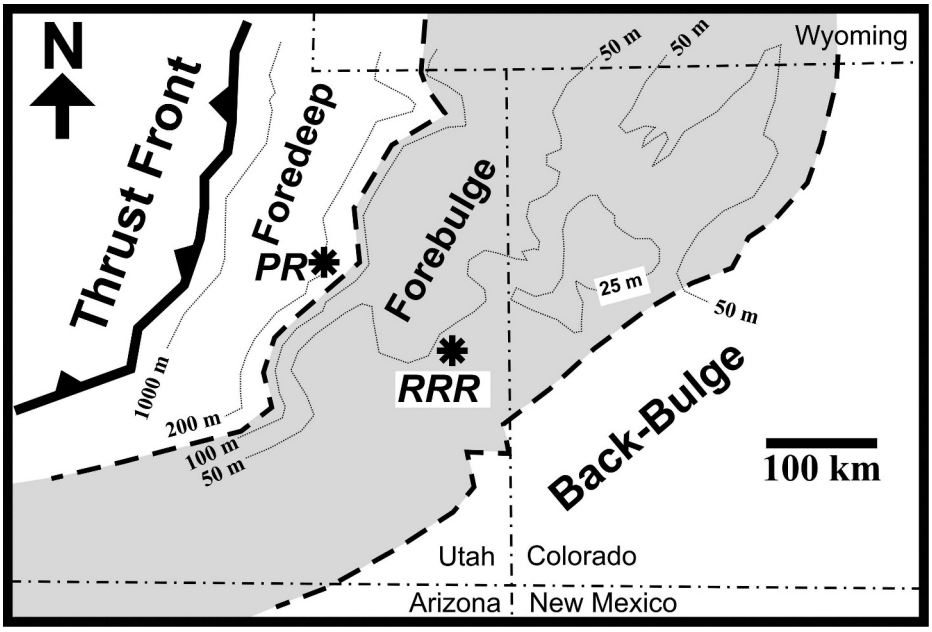

FIG. 3.—Isopach map of Lower Cretaceous strata and generalized paleogeographic map of the Sevier thrust front and foreland-basin system in Utah and Colorado during the Albian, modified from Currie (2002). Note location of the Price River (PR) section in the area of the foredeep, and location of the Ruby Ranch Road (RRR) section in the area of the forebulge.

washed with water, and oven dried to evaporate all liquid residues. Slabs were subsequently vacuum-impregnated, micropolished, and archived with their counterpart ends for fabric analysis and stable-isotope microsampling.

The chemostratigraphy of micritic to microsparitic nodular carbonates sampled from the Price River section was evaluated by averaging five microanalysis samples ($\sim$ 0.5 mg) of fine-grained carbonate milled from polished slabs using a microscope-mounted microdrill assembly using 0.5 mm dental bits. The carbonate chemostratigraphy of the Ruby Ranch Road section was evaluated using stratigraphic sampling procedures outlined in Ludvigson et al. (2004), by milling $\sim$ 1 g of powdered micritic calcite from slabbed surfaces for coordinated carbonate and organic carbon isotope data, using 7.5 mm dental bits.

Calcite microsamples of 20–30 micrograms were roasted *in vacuo* for 1 hr at 380° C to remove volatiles, and reacted with anhydrous H_3PO_4 at 70° C in an automated Kiel III device coupled to a ThermoFinnigan MAT 252 stable-isotope mass spectrometer (Price River; analyzed at the University of Iowa) or ThermoFinnigan MAT 253 stable-isotope mass spectrometer (Ruby Ranch Road; analyzed at Keck Paleoenvironmental and Environmental Stable Isotope Laboratory, University of Kansas). Results are reported relative to the VPDB isotope standard, with precision of $\delta^{13}C$ and $\delta^{18}O$ values better than $\pm$ 0.1‰.

Petrographic and Diagenetic Evaluations

A selected subset of the chemostratigraphic rock samples collected for this study were cut into matching micropolished thin and thick sections to evaluate their petrography and carbonate micromorphology. These samples were examined by polarized light and cathodoluminescence microscopy. For some of these samples, petrographic inventories of carbonate components were undertaken to guide more intensive carbon and oxygen isotopic microsampling efforts in order to define characteristic diagenetic trends in $\delta^{13}C$ and $\delta^{18}O$ isotope space. Well-defined diagenetic trends have specific genetic connotations for discriminating products of early and late diagenesis in carbonate rocks, and they were applied in this study following orthodox interpretations of carbonate diagenesis. Moreover, the characterization of component-specific diagenetic trends can clarify the genetic origins of chemostratigraphic structure (Ludvigson et al. 1996).

U-Pb Dating of Carbonate Rock at Ruby Ranch Road Section

A brecciated micritic limestone with high U contents based on phosphor imaging (Cole et al. 2003) was discovered near the boundary between the Yellow Cat and Poison Strip Sandstone members at the Ruby Ranch Road section. Microsampling of this limestone was guided by phosphor imaging, which indicated U enrichment in a gray micrite phase. The microsampled powders were treated using techniques similar to those of Cole et al. (2005). Samples were run on outgassed Re filaments in static mode with a Finnigan MAT 262 at Stony Brook University. Data were corrected for mass fractionation of 0.08 $\pm$ 0.04 per amu based on multiple runs of NBS 982. The U and Pb blanks were less than 100 picograms and are negligible in these high Pb and U concentration samples. The programs PbDat and IsoExcel (Ludwig 2003) were applied to the data.

U-Pb Dating of Detrital Zircons at Ruby Ranch Road Section

Detrital-zircon sample preparations followed procedures outlined by Gehrels et al. (2006). Approximately 100 single-grain U-Pb ages ($^{206}Pb/^{238}U < \sim 1.0$ Ga $> {}^{206}Pb/^{207}Pb$) were determined for each of two rock samples from the Ruby Ranch Road section utilizing a New Wave DUV193 LA-MC-ICPMS at the Arizona LaserChron Center, University of Arizona (Gehrels et al. 2006). Analytical results are presented using features available in Ludwig (2003). Maximum depositional ages were determined from age-error (2σ) overlap of at least three of the seven youngest grains in each sample using the TuffZirc algorithm of Ludwig (2003).

RESULTS

Coeval Successions Yielding Chemostratigraphic Records

We made systematic observations on the lithologic characteristics of the Cedar Mountain Formation at two sections, thereby greatly refining the accounts provided by previous authors and providing the most complete stratigraphic context for the terrestrial authigenic carbonates heretofore available. Thus, the resultant record of Cretaceous CIEs from the Cedar Mountain Formation (CMF) can be accurately placed within stratigraphic, sedimentologic, and diagenetic contexts. We do not provide

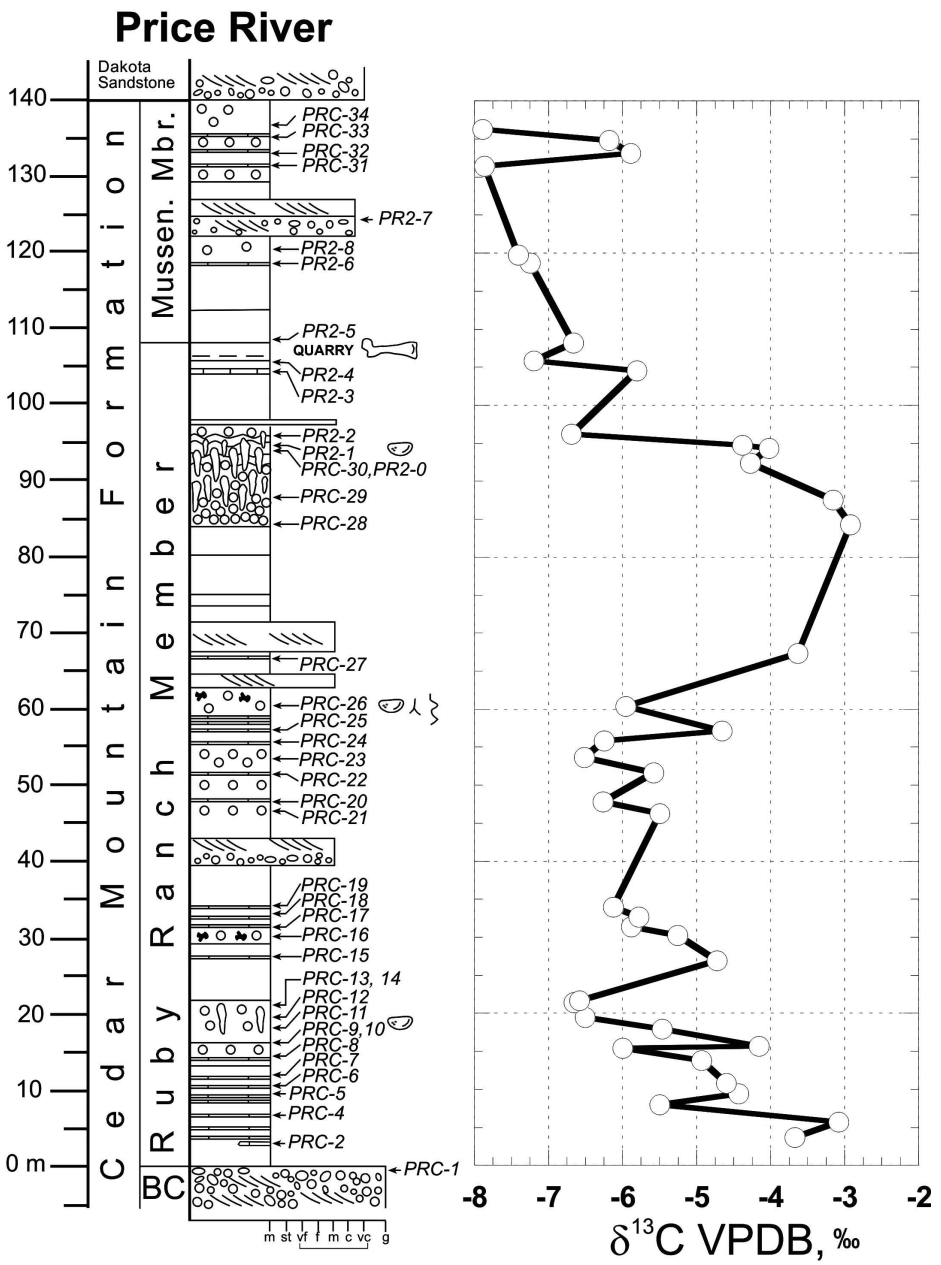

FIG. 4.—Graphic log of the lithostratigraphy and carbonate $\delta^{13}C$ chemostratigraphy of the Price River section. The identities and positions of chemostratigraphic samples are shown on the right side of the graphic log. (see Fig. 8 for symbol key).

a lithofacies analysis of the CMF, however, because our chief purpose has been to secure chemostratigraphic profiles from nodular carbonates (''calcretes'') alone.

Price River Section (PR).—At Price River (Fig. 4), the Buckhorn Conglomerate is overlain by the Ruby Ranch Member, which is subsequently overlain by the Mussentuchit Member. The Ruby Ranch Member at Price River is nearly 100 m thick, more than double the thickness of equivalent strata at Ruby Ranch Road (see forthcoming section). Approximately 90% of the Ruby Ranch Member at Price River consists of massive, noncalcareous to calcareous, reddish to greenish-gray mudstones. Color gradations (e.g., from high-chroma reddish to reddish brown colors to low-chroma greenish or grayish colors) across nondepositional pedogenic or geochemical boundaries are common in these mudstones. Likewise, mottling appears in some horizons. Ruby Ranch Member mudstones weather into fine to medium blocky structure and in some horizons exhibit small polished faces and small to medium slickensides of probable pedogenic origin. Many horizons and of distinct to intergrown, irregular, spheroidal to cylindroidal (i.e., vertically elongate) nodules of micritic to microsparitic calcite are distributed throughout the mudstones of the Ruby Ranch Member (Fig. 5A, B). Most of these horizons are 0.1–1.5 m in thickness, but a particularly thick (12.1 m) horizon of large carbonate nodules within massive reddish-brown mudstone lies at the top of the Ruby Ranch Member at Price River (Figs. 4, 5A). This horizon is a prominent marker that can be traced laterally across the nearby area. There are vague long-amplitude structures in this thick nodule-bearing horizon that may be analogous to ''pseudoanticlines'' described from petrocalcic horizons that formed below modern land surfaces in drier climates (cf. Jennings and Sweeting 1961; Watts 1977; Goudie et al. 1990). Features found in carbonate nodules and beds in the Ruby Ranch Member include blocky-spar-filled circumgranular cracks and engulfed small nodules (Fig. 6), void-filling

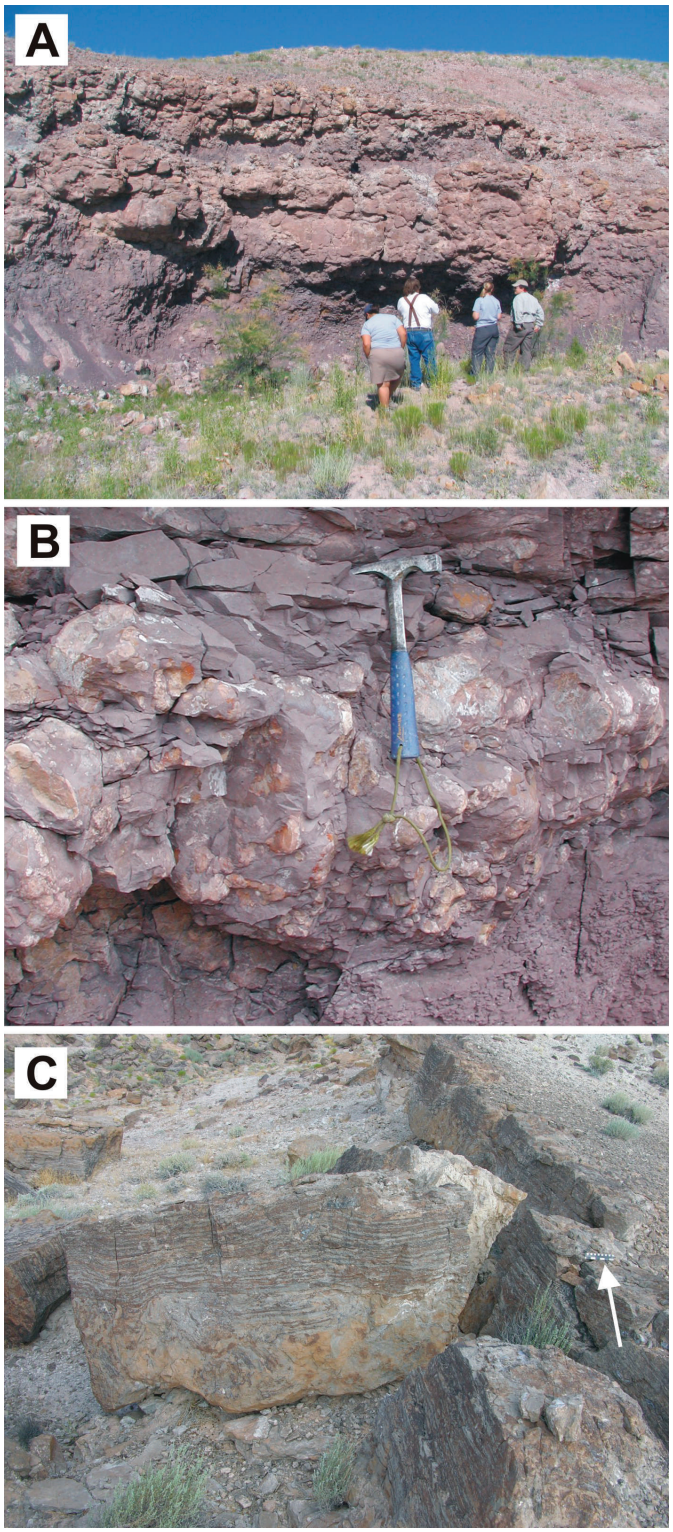

FIG. 5.—Field photographs of nodular carbonates "calcretes" in the Cedar Mountain Formation. **A)** Massive "calcrete" bed at the 84 to 97 meter level in the Price River section (Fig. 4). Geologists for scale. **B)** Coalesced spheroidal nodules of micritic calcrete at the 95 meter level in the Price River section (Fig. 4). Geologic hammer for scale. **C)** Block of 1.1-meter-thick "calcrete" bed at the position of RRR-7 (base) and RRR-8 (top) in the Ruby Ranch Road section (Fig. 8). Note brecciated laminated fabric. White arrow points toward centimeter/inch scale bar.

chalcedony, ostracodes (Fig. 7), probable root traces, and millimeter-scale burrows. Approximately 10% of the thickness of the Ruby Ranch Member at Price River consists of thin, medium to coarse cross-bedded sandstones.

The Mussentuchit Member is approximately 40 m thick at Price River, and consists of nearly 90% massive, reddish to light gray and light greenish gray mudstone and, at the very top of the member, fissile shale (Fig. 4). In general, lower-chroma (greenish to grayish) colors dominate in an upward trend through the member. Micritic to microsparitic calcite nodules and horizons or beds of coalesced nodules, very similar to those in the Ruby Ranch Member, appear in the Mussentuchit Member at Price River (Figs. 4, 6A).

The Dakota Sandstone unconformably overlies the Mussentuchit Member at Price River, and it consists of trough cross-bedded, matrix-supported, pebble to cobble conglomerate.

Ruby Ranch Road Section (RRR).—At Ruby Ranch Road, the type Ruby Ranch Member is exposed atop the Poison Strip Sandstone (Fig. 8), which overlies a thick section of the Yellow Cat Member (Kirkland and Madsen 2007). The Poison Strip Sandstone consists of massive and planar-laminated, medium to very coarse and gravelly, lithic sandstones with minor silty mudstone. Horizontal to subvertical burrows and bioturbation are apparent at multiple levels. Sandstones in the Poison Strip Sandstone here typically have poikilotopic calcite cements.

In the lower Poison Strip Sandstone, at the position of samples RRR-7 to RRR-8 (Fig. 8), is a 1.1-meter-thick brecciated laminar and chalcedony-replaced micritic limestone (Fig. 5C). The unit contains wavy stromatolitic laminae at the decimeter scale. This unit is traceable over distances of several kilometers at the Ruby Ranch Road section, and has been interpreted to be a shallow lacustrine limestone (Kirkland and Madsen 2007). This unit yields the early Aptian U-Pb date described elsewhere in this paper.

Approximately 75% of the Ruby Ranch Member at Ruby Ranch Road consists of mudrocks, dominantly massive, calcareous to noncalcareous, reddish to greenish-gray mudstones, silty mudstones, and siltstones; shales (i.e., fissile mudrocks) are a very minor component, being prominent only at the top of the member. These mudstones weather into fine to medium blocky structure. Mottling is prominent in some of the massive mudstones and siltstones. Small (millimeter- to centimeter-scale) to large (decimeter-scale) and irregularly shaped nodules of micritic to microsparitic calcite are common in mudrocks throughout the Ruby Ranch Member at Ruby Ranch Road. Approximately one-quarter of the Ruby Ranch Member's aggregate thickness at Ruby Ranch Road comprises sandy siltstone and silty very fine sandstone, the latter containing chert pebbles.

The Dakota Formation unconformably overlies the Ruby Ranch Member at Ruby Ranch Road, and it consists of trough cross-bedded, very coarse pebbly sandstone and matrix-supported pebble conglomerate.

Petrography of Nodular Carbonates ("Calcretes").—In carbonate nodules from the Cedar Mountain Formation, we observe: (1) small nodules of secondary micritic to microsparitic carbonate within pedogenically modified mudstones; (2) larger, spheroidal, cylindroidal, and irregularly discoidal nodules of micritic to macrosparitic carbonate that occur commonly at discrete levels in successions of mudstones; and (3) beds of coalesced nodules of the formerly described type.

Carbonate nodules in the Cedar Mountain Formation are distinguished by a discrete set of micromorphological features: (1) dense groundmass of micritic to microsparatic calcite, equivalent to the crystallitic b-fabric of soil micromorphology (Stoops 2003); (2) included, millimeter-to-centimeter-scale nodules of micritic to microsparitic carbonate, equivalent to typic nodules (Stoops 2003); (3) spar-filled circumgranular cracks; and (4) included grains of quartz silt and sand

floating in the carbonate groundmass. There are also salient patterns in the cathodoluminescence (CL) of these authigenic carbonates. The dense groundmass of micritic to microsparitic calcite in "calcretes" of the Cedar Mountain Formation is always brightly luminescent overall, but it also appears as a distinctively heterogeneous speckled mosaic at the scale of tens of microns (Fig. 6B, C). In contrast, blocky equant calcite spars filling circumgranular cracks contain an early generation of nonluminescent spar followed by subsequent generations of luminescent calcites. (Fig. 6B, C). Small nodules included within the carbonate groundmass are generally luminescent but vary individually in their CL intensity. Some of these nodules are less luminescent than the enclosing carbonate matrix.

Features indicating a dominance of vadose pedogenic processes are utterly absent in the Cedar Mountain Formation "calcretes." Such features would include fine-grained carbonate in the forms of concentric (pisolitic) nodules and continuous multilayered laminar coatings, solutional pipes, and evidence for the progressive plugging of soil pores by carbonates, sequential evolutionary stages in soil calcic or petrocalcic horizon development, or repeated episodes of vadose dissolution and recementation. Such features would be expected in a petrocalcic (e.g., Bkm) horizon, that is, a calcrete defined in the narrowest pedological sense.

Whereas evidence for a dominance of vadose processes is lacking in the Cedar Mountain Formation "calcretes," ostracodes, charophytes, and nonmarine gastropods, indicative of shallow ponded freshwater environments, appear in approximately 20% of the petrographic thin sections examined by our studies (Fig. 7).

Carbonate Carbon Isotope Chemostratigraphy

Price River Section (PR).—The general trend of the carbon isotope profile at Price River is one of a long-term fall from peak $\delta^{13}C$ values of about −3‰ down to about −8‰ VPDB (Fig. 4). Carbonate $\delta^{13}C$ values in the lower half at Price River have baseline of about −6‰ VPDB. At two positions, $\delta^{13}C$ values rise up to peak values of about −3‰, at about the 6 m and 84 m stratigraphic levels (Fig. 4). The upper peak occurs as part of a long-ranging, broad positive carbon isotope excursion (CIE) between the 60 m level and the top of the Ruby Ranch Member (Fig. 4). The $\delta^{13}C$ values continue to decrease upward through the Mussentuchit Member to values as low as −8‰ VPDB, but a more short-term positive CIE with peak $\delta^{13}C$ values of approximately −6‰ appears just below the Dakota Sandstone (Fig. 4; 131–136 m interval).

Ruby Ranch Road Section (RRR).—The chemostratigraphic profile from the Ruby Ranch Road section is similar to that at Price River, and shows a long-term fall from peak $\delta^{13}C$ values of about −3‰ down to values lower than −6‰ VPDB (Fig. 8). Higher $\delta^{13}C$ values appear in two peaks of about −3‰ VPDB near the 3 m and 37 m stratigraphic levels (Fig. 8). At Ruby Ranch Road, the peaks are part of two discrete positive CIEs, one at approximately the 0 to 7 m level, and the other at the 33 to 40 m levels (Fig. 8).

The $\delta^{13}C$ values in the lower positive CIE peak in the Poison Strip Sandstone in the Ruby Ranch Road section (Fig. 8) are very similar to values from lacustrine oncoids reported from an equivalent stratigraphic interval (Shapiro et al. 2009).

Diagenetic Trends and Stable-Isotope Variability of Nodular Carbonates ("Calcretes").—Carbonate components in samples PRC-23 and PRC-10 include micritic matrix calcites and calcitic microspars, calcite spars filling intergranular pores in intraclastic packstones, and vein calcites (Fig. 9). The isotopic variations in these components can be used to define diagenetic trends in carbon-oxygen isotope space that are characteristic of these individual components, and to thus interpret the diagenetic and paleohydrologic processes recorded by those components, following orthodox interpretations of carbonate diagenesis (James and Choquette 1990; Choquette and James 1990).

The full complement of carbonate components in rock sample PRC-23 have $\delta^{13}C$ values that range between −7.6 and −5.8‰ VPDB, and $\delta^{18}O$ values that range between −10.3 and −7.9‰ VPDB (Fig. 9). Carbonate components from rock sample PRC-10 have $\delta^{13}C$ values that range between −6.4 and −3.5‰ VPDB and $\delta^{18}O$ values that range between −11.3 and −7.7‰ VPDB (Fig. 9). The matrix micritic and microsparitic calcites, however, have much less variable $\delta^{18}O$ values. Isotopic data from the fine-grained matrix carbonates are arrayed along vertical linear trends that are referred to as "*meteoric calcite lines*" (*sensu* Lohmann 1988; James and Choquette 1990; M.B. Suarez et al. 2009), and labeled as "MCL" in Figure 9. Sample PRC-23 yielded an average MCL $\delta^{18}O$ of −8.1‰ (s.d. = 0.16‰), and sample PRC-10 yielded an average MCL $\delta^{18}O$ of −8.0‰ (s.d. = 0.17‰). In contrast to the fine-grained matrix calcites, the intergranular spar and vein calcites have lighter and more variable $\delta^{18}O$ values that are arrayed along a horizontal diagenetic trend in carbon–oxygen isotope space (Fig. 9).

U-Pb Date from Limestone at Ruby Ranch Road

Five microsampled aliquots of uranium-enriched micritic calcite were milled from an internal polished slab of the rock sample from the position of RRR-8 (Fig. 8). Based on the purity of this micritic limestone in thin-section view, and the lack of solid residues in the dissolved aliquots, the U and Pb contents in this rock are bound in calcite. U concentrations range from 114 to 592 ppm, Pb concentrations of 3.9 to 44 ppm, and $^{238}U/^{204}Pb$ from 283 to 7429. The radiogenic U-Pb isotopes in this rock indicate that it formed in the early Aptian Stage at about 119.4 ± 2.6 Ma. The five aliquots give a Total Pb-U age of 119.4 ± 2.6 Ma with a mean square of weighted deviates (MSWD) of 7.5 while the ^{238}U-^{206}Pb isochron ages is 119.47 ± 0.75 Ma with a MSWD of 0.56; the Pb-Pb age is 120 ± 58 Ma with a MSWD of 18 (Table 1). The coherency of the U-Pb and Pb-Pb ages suggests that the ages are reliable within the stated uncertainty of the Total Pb-U age.

U-Pb Dates from Detrital Zircons at Ruby Ranch Road

Detrital zircon U-Pb ages (Fig. 10) from the Poison Strip Sandstone (sample RRR-12; n = 93) corroborate current interpretations of a dominant source in the Sevier fold-thrust belt mixed with other sources, including basement rocks in the Mogollon Highlands (Dickinson and Gehrels 2008). The Buckhorn Conglomerate of the Cedar Mountain Formation and the Burro Canyon Formation localities display a high degree of overlap with the Poison Strip Sandstone (Fig. 11).

Detrital-zircon age populations in the Dakota Sandstone (sample RRR-54) are comparable with those found in Neoproterozoic quartzites from Sevier allochthons (Hunt and Lawton 2008), with the addition of ages characteristic of ubiquitous Permian–Jurassic eolian sandstones (Dickinson and Gehrels 2003). Only two Yavapai–Mazatzal (1800–1600 Ma) grains were sampled in RRR-54, suggesting limited input from Mogollon Highlands basement and a reduced role for recycled Cambrian–Permian continental-shelf strata and Mesozoic erg strata in the thrust belt, all of which have prominent peaks of this age (Dickinson and Gehrels 2008). Hunt and Lawton (2008) reported very few Yavapai–Mazatzal grains in the Neoproterozoic Caddy Canyon Quartzite in central Utah, in conflict with the interpretations of Lawton and Willis (1987) and Sprinkel et al. (1999). The Tintic/Prospect Mt. Quartzite in the Canyon Range allochthon is notable for having a dominant Yavapai–Mazatzal peak (Hunt and Lawton 2008), suggesting that Cambrian, and perhaps most thrust-belt strata in general, were a limited local source during the deposition of the Dakota Sandstone. Instead, sources originating in the Cordilleran arc appear to dominate the Dakota. The Dakota Sandstone further contrasts with the Poison Strip Sandstone in containing a much higher percentage of Mesozoic arc-derived grains, particularly Cretaceous ones (Fig. 12).

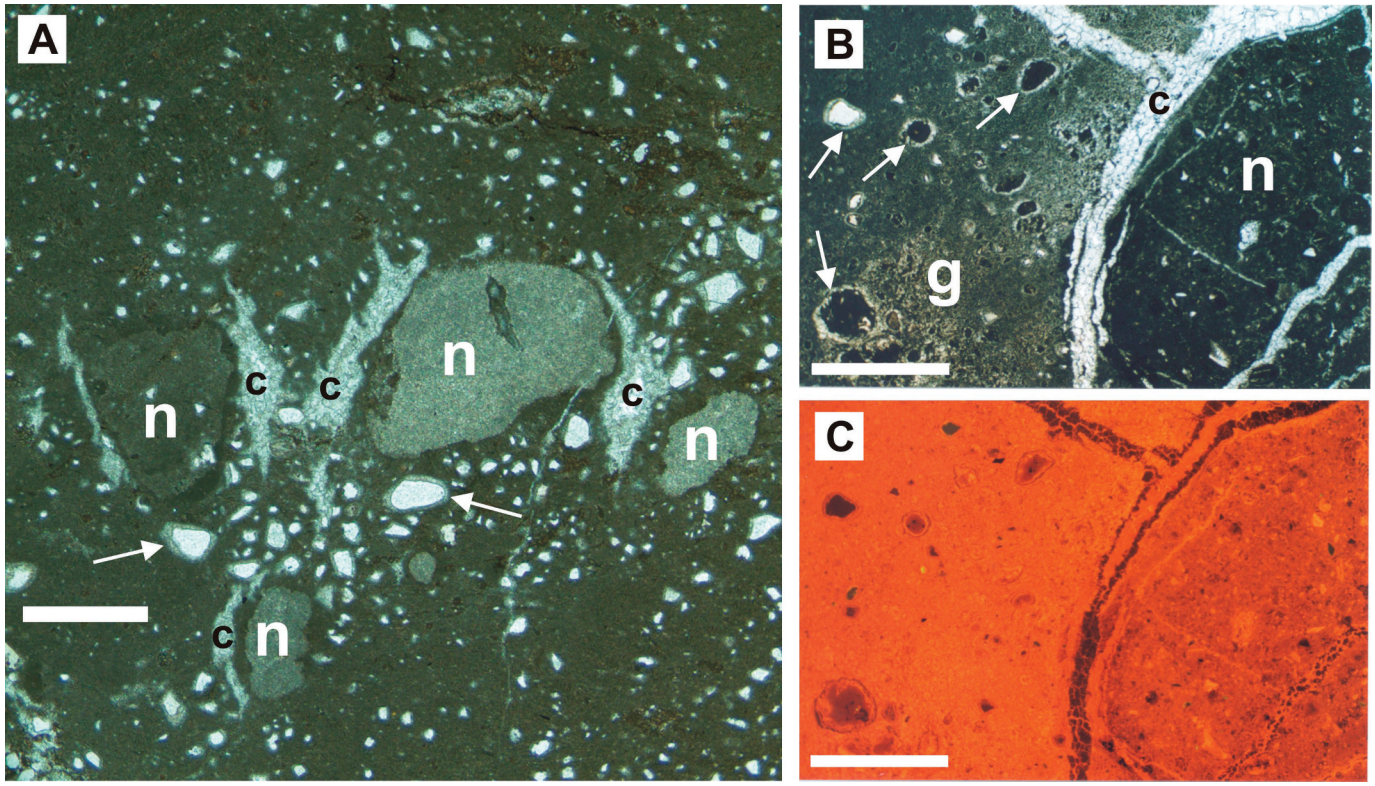

FIG. 6.—Micromorphology of nodular carbonates ("calcretes") of palustrine origin from the Cedar Mountain Formation. **A)** Dense groundmass of micritic carbonate (crystallitic b-fabric). Nodules (n) of micrite and microspar engulfed in groundmass, spar-filled circumgranular cracks (c), floating quartz silt and sand grains (white), (white arrows). Rock sample PRC-31 at the 132-meter-level in the Price River section (Fig. 4). Plane-polarized light; scale bar is 1 millimeter in length. **B)** Contrasting micromorphologies of matrix calcites. Dense micritic carbonate in nodule to right (n), and microsparitic carbonate in groundmass to left (g), with intervening spar-filled circumgranular crack (c). Note nodules partially to completely surrounded by circumgranular cracks (white arrows). Transmitted light; scale bar is 1 millimeter in length. Rock sample PR2-4 at the 105-meter-level in the Price River section (Fig. 4). **C)** Same field of view as in Part B, under emitted cathodoluminescence (Nuclide ELM-2 at 10 kV and 0.5 mA electron beam). Note fine-scale speckled mosaic of nonluminescent and luminescent calcite domains at the scale of tens of microns in the micritic nodule to right. In contrast, note the more uniformly luminescent speckled mosaic in the microsparitic groundmass to the left. The calcite spar filling the circumgranular crack has an early nonluminescent zone followed by a luminescent zone. Note early generation of nonluminescent spar in circumgranular cracks around nodules. Scale bar is 1 millimeter in length.

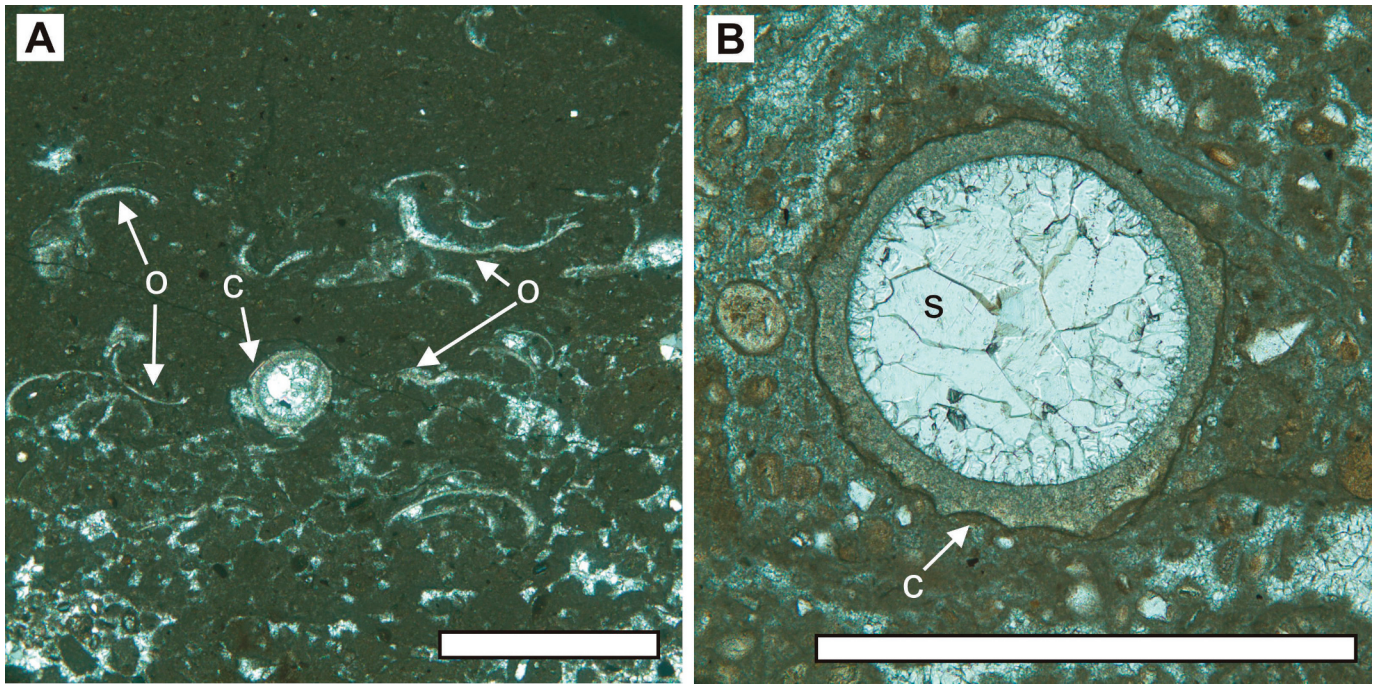

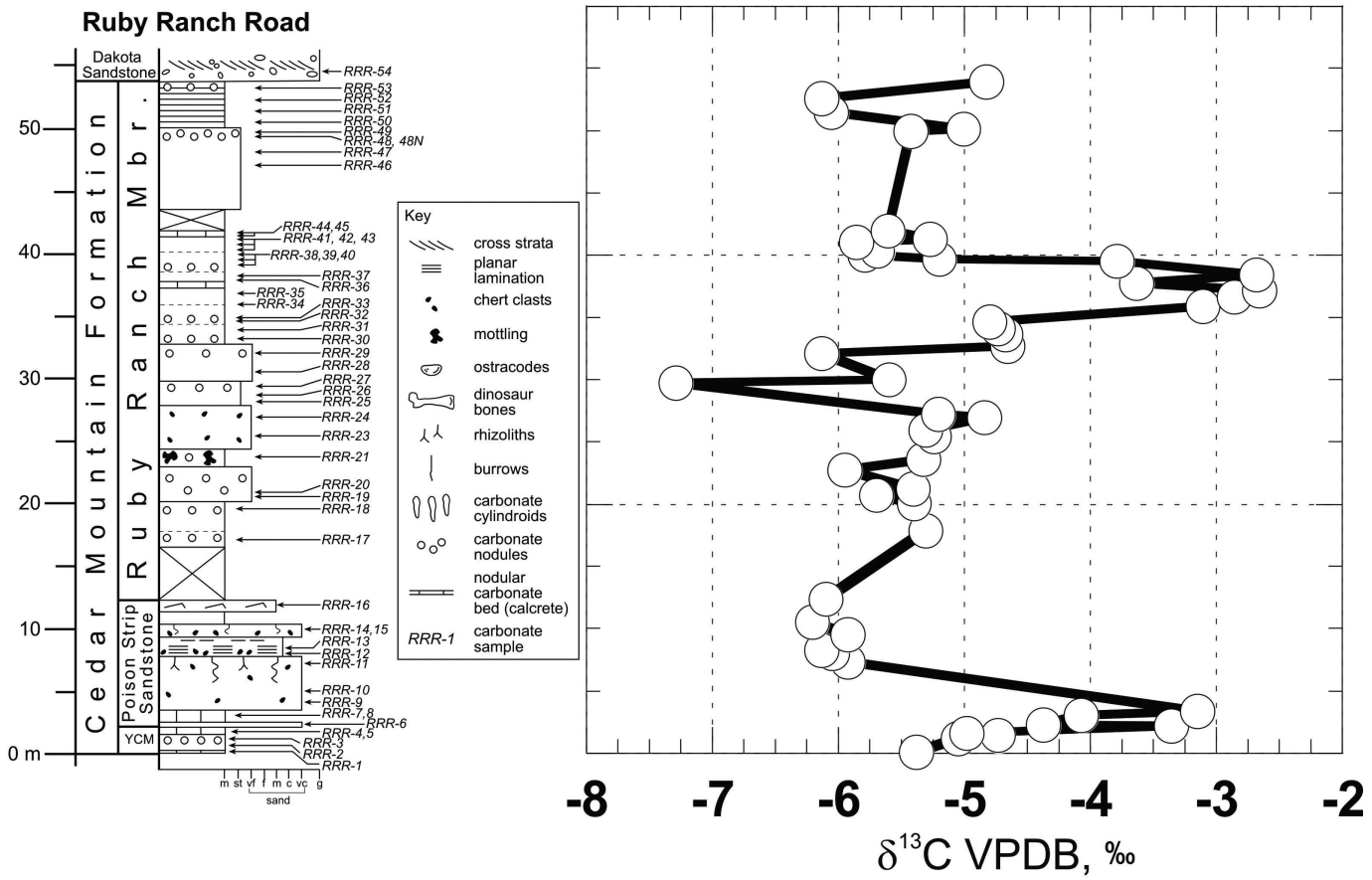

FIG. 8.—Graphic log of the lithostratigraphy and carbonate $\delta^{13}C$ chemostratigraphy of the Ruby Ranch Road section. The identities and positions of the chemostratigraphic samples are shown on the right side of the graphic log.

DISCUSSION

Origins of Nodular Carbonates ("Calcretes")

Interpretation of Primary Processes and Depositional Environments.— The nodular carbonates of the Cedar Mountain Formation are not, as a whole, vadose soil features like petrocalcic horizons. Our application of the term "palustrine" to these carbonates is prompted by their inclusion of characteristic aquatic fossils. Nonetheless, the carbonates also contain features indicative of vadose processes, such as autobrecciation, meniscate cements, and circumgranular cracks. Syndepositional phreatic groundwater recrystallization of the carbonates was pervasive and determined their net petrographic and geochemical characteristics. The stable-isotope record of the Cedar Mountain Formation carbonates was formed by multiple near-surface processes. These processes were syndepositionally integrated through soils and sediments below successive Cretaceous land surfaces in the aggrading foreland basin.

Salient early diagenetic signatures in CMF calcretes are verified through: (1) documentation of cathodoluminescence patterns related to time-averaged meteoric diagenesis; (2) identification of meteoric calcite line (MCL) diagenetic trends in carbon–oxygen isotope space (Lohmann 1988); (3) discrimination of individual MCLs in specific stratigraphic horizons by their unique ranges of $\delta^{13}C$ values; (4) corroboration of MCL-derived $\delta^{18}O$ water values by phosphate-derived $\delta^{18}O$ water values from fossil semiaquatic vertebrates; and (5) differentiation of later diagenetic trends in carbon–oxygen isotope space that are distinctly different from the MCLs.

Diagenetic Analysis.—The micritic and microsparitic groundmass of so-called calcretes in the Cedar Mountain Formation uniformly displays bright cathodoluminescence (CL) in a heterogeneous speckled mosaic pattern of luminescent and nonluminescent calcite domains that are developed at the scale of tens of microns (Fig. 6B, C). Bright CL luminescence in calcite is typically related to Mn^{2+} activation by

←

FIG. 7.—Typical carbonate fabrics and fossils diagnostic of aquatic environments in nodular carbonates of palustrine origins from the Ruby Ranch Member of the Cedar Mountain Formation. **A)** Ostracode (o) wackstone to packstone containing single charophyte (c), cross-polarized light, scale bar is 1 mm. **B)** Charophyte grain (c) from peloidal grainstone in another "calcrete" nodule; note included sand and silt grains in micritic to microsparitic carbonate matrix, and internal fill of calcite spar (s) within charophyte, plane-polarized light, scale bar is 1 mm.

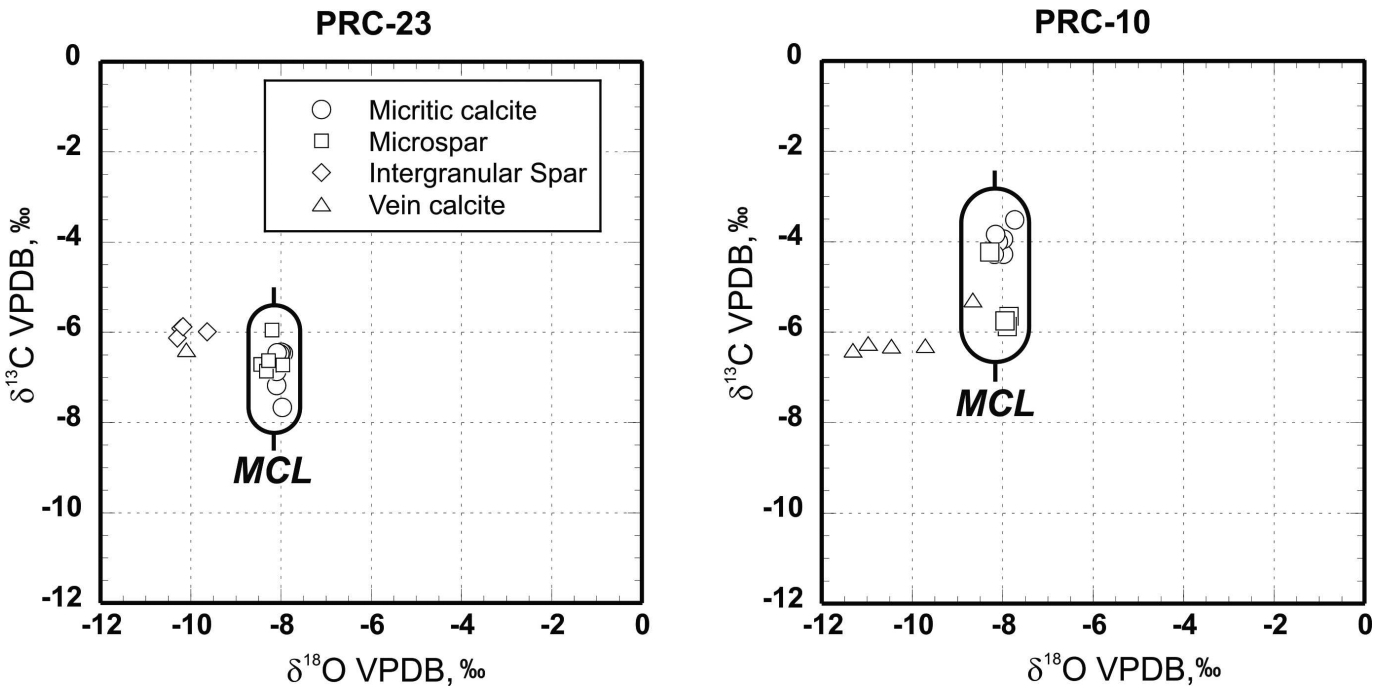

FIG. 9.—Carbon and oxygen isotope plots showing $\delta^{13}C$ and $\delta^{18}O$ values measured from carbonate components in rock samples PRC-23 and PRC-10. See Figure 4 for the positions of these samples. The symbols MCL denote the vertical linear trends of meteoric calcite lines that are characteristic of the authigenic micritic and microspar calcites in these samples.

precipitation from reducing meteoric phreatic groundwaters (Boggs and Krinsley 2006, p. 124–125).

The micron-scale juxtaposition of luminescent and nonluminescent domains indicates that fine-grained calcite crystallized in multiple diagenetic environments. Luminescent domains typically crystallize from reducing meteoric phreatic pore fluids, whereas nonluminescent domains typically crystallize from oxidizing pore fluids (Boggs and Krinsley 2006). Such a CL mosaic likely results from the original microscopic juxtaposition of diagenetically resistant low-magnesium calcite (LMC) with high-magnesium calcite (HMC) and aragonite (A)—polymorphs that are more susceptible to diagenetic alteration (James and Choquette 1990, p. 41). HMC and A originally precipitate from evaporatively concentrated vadose pore fluids with higher ionic concentrations than those that precipitate LMC. Later, when HMC and A are bathed in more dilute meteoric phreatic pore fluids, they recrystallize to LMC. Thus, we interpret the pervasive CL mosaic in "calcretes" of the Cedar Mountain Formation as the result of partial early diagenetic recrystallization by syndepositional meteoric phreatic pore fluids (cf. Budd et al. 2002). Such recrystallization, in effect, yields a time-averaged record of paleoclimate because noncontemporaneous vadose and phreatic components are preserved together. Likewise, palustrine carbonates cannot yield highly resolved ($< 10^4$ years) records of paleoenvironmental change because their records of early vadose and phreatic diagenesis are integrated, and therefore time-averaged. Cojan et al. (2000), however, demonstrated that Maastrichtian–Lutetian palustrine carbonates record global CIEs at scales of 10^5 to 10^6 years, and therefore Aptian–Albian CIEs should be resolvable from the Cedar Mountain Formation "calcretes."

TABLE 1.—*Uranium-lead dates on rock sample RRR-8.*

Type of Isochron	Age (2σ uncert) Ma	MSWD
Total Pb-U	119.4 (2.6)	7.5
$^{238}U/^{204}Pb$ versus $^{206}Pb/^{204}Pb$	119.47 (0.75)	0.56
$^{207}Pb/^{204}Pb$ versus $^{206}Pb/^{204}Pb$	120 (58)	18

Fine-grained matrix carbonates in rock samples PRC-23 and PRC-10 produce isotopic data that are arrayed along *meteoric calcite lines* (MCLs) (Fig. 8). MCLs are vertical diagenetic trends in carbon–oxygen isotope space that are characterized by relatively invariant $\delta^{18}O$ values and more variable $\delta^{13}C$ values (Lohmann 1988; James and Choquette 1990, p. 61–62). MCLs preserve isotopic records of calcite crystallization in early meteoric diagenetic environments, and they are proxies for paleoprecipitation (Lohmann 1988; M.B. Suarez et al. 2009). The MCL values determined from rock samples PRC-23 and PRC-10 are -8.1 ± 0.16‰ and -8.0 ± 0.17‰ VPDB, respectively. These values closely match two other MCL values of -7.5 and -8.0‰ VPDB that were independently determined from two other rock samples from the Cedar Mountain Formation (see Ludvigson et al. 2003; M.B. Suarez et al. 2009). MCL estimates of the $\delta^{18}O$ values of paleoprecipitation from the Cedar Mountain Formation were stable over long stratigraphic ranges, and yield zonal mean groundwater $\delta^{18}O$ estimates of about -6‰ VSMOW for Aptian–Albian locales at 34° N paleolatitude (M.B. Suarez et al. 2009).

This estimated depositional $\delta^{18}O$ groundwater value for the CMF is fully consistent with synsedimentary Cretaceous surface-water $\delta^{18}O$ estimates derived from turtle scutes and crocodile tooth enamel from the Price River 2 Dinosaur Quarry (Fig. 4) in the Ruby Ranch Member (C.A. Suarez 2010). The vertebrate phosphate water $\delta^{18}O$ estimates were derived using taxon-specific equations (Barrick et al. 1999; Amiot et al. 2007). Water $\delta^{18}O$ estimates from carbonates (-5.6 ± 0.6‰ VSMOW), turtles (-7.3 ± 0.8‰ VSMOW), and crocodiles (-5.0 ± 0.3‰ VSMOW) at the quarry are mutually consistent (C.A. Suarez 2010, p. 129), given certain considerations. Carbonate and crocodile water $\delta^{18}O$ estimates likely reflect influences of local evaporative enrichment of fluid ^{18}O relative to values derived from fossil turtles (C.A. Suarez 2010), which are regarded as excellent proxies for local surface water $\delta^{18}O$ values (Barrick et al. 1999). The mutual consistency between these paleohydrologic proxies unequivocally demonstrates that the MCL values

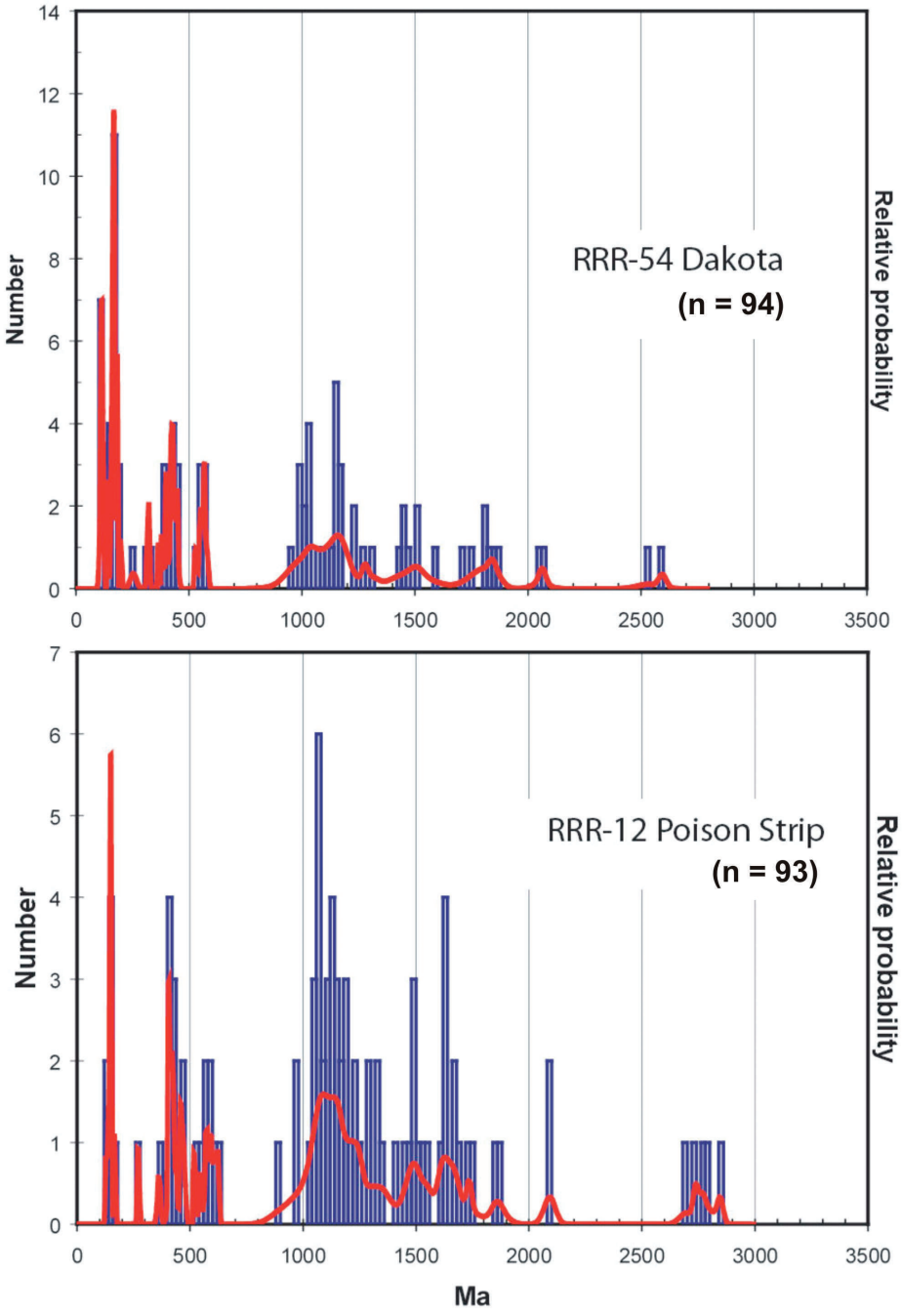

FIG. 10.—Age-bin histograms and age-distribution curves of U-Pb dates for the complete populations of detrital zircon grains from sandstone samples RRR-12 and RRR-54 at the Ruby Ranch Road section, shown in Figure 4.

derived herein from the CMF (Fig. 9) are, in fact, products of early meteoric diagenesis.

During the initial phase of stable-isotope microsampling of the chemostratigraphic profile at Price River (Fig. 4), the average standard deviation from the mean $\delta^{13}C$ values from the 40 stratigraphic samples of fine-grained carbonates was 0.36 per mil. The total range in mean $\delta^{13}C$ values through the entire chemostratigraphic profile is ~ 5 per mil (Fig. 4). Therefore, the intrinsic variability in $\delta^{13}C$ values within each rock sample is about an order of magnitude less than that of the total stratigraphic variation, and the chemostratigraphic profile represents a record of real stratigraphic changes in $\delta^{13}C$, rather than simply being an artifact of high intrinsic variability in the samples.

During the additional microsampling of carbonate components from PRC-23 and PRC-10 (Fig. 9), further data were accumulated on the intrinsic isotopic variability of fine-grained carbonates by expanding the sampling frequency from the initial number of five microsamples upwards to 18 (PRC-23) and 15 (PRC-10). These additional microsamples changed the mean $\delta^{13}C$ value from rock sample PRC-23 from an initial determination of $-6.5 \pm 0.17‰$ to an updated determination of $-6.7 \pm 0.41‰$, and from rock sample PRC-10 from an initial determination of $-4.1 \pm 0.43‰$ to an updated determination of $-4.5 \pm 1.5‰$. The initial ($n = 5$) and more extensive microsampling ($n = 15$ to 18) produced compatible results, further confirming that these are real stratigraphic changes in $\delta^{13}C$ values.

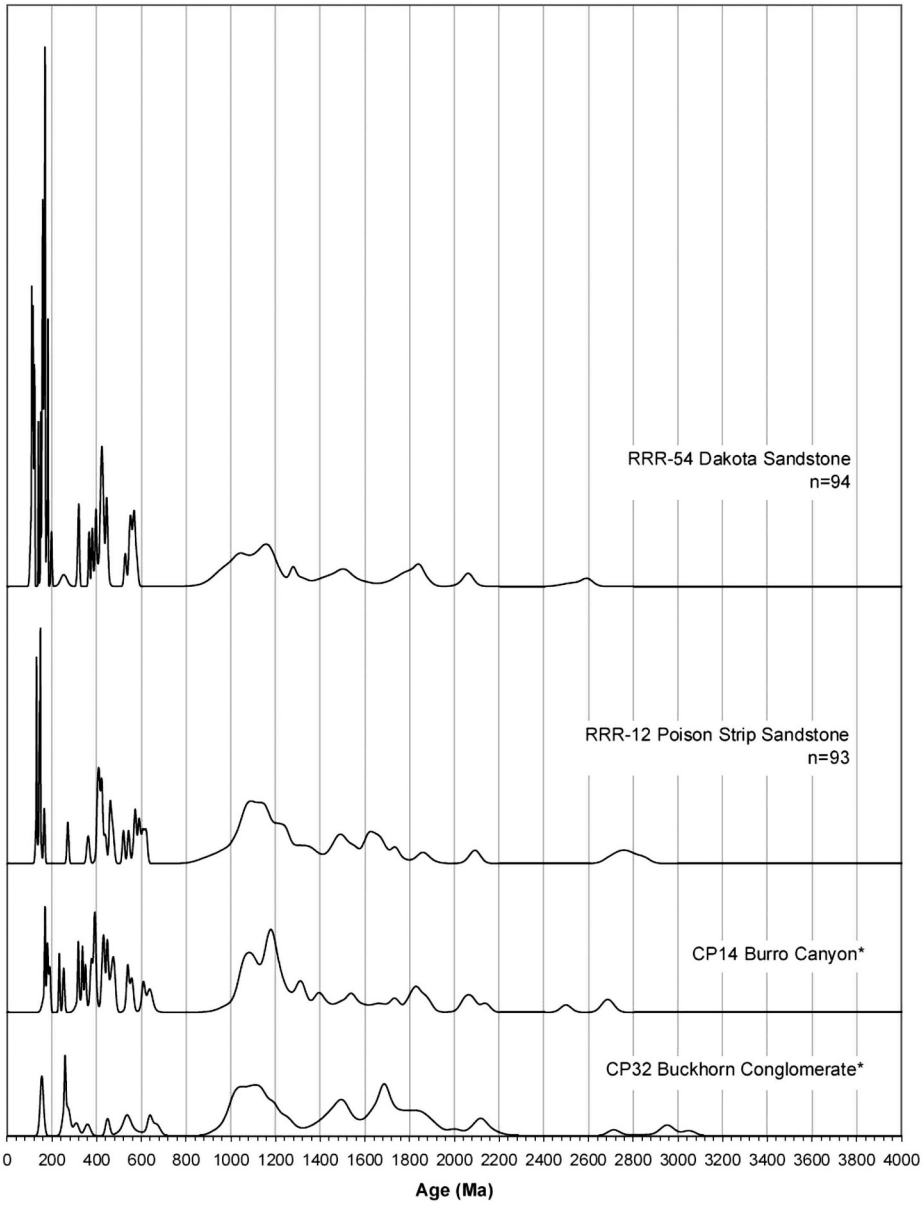

FIG. 11.—Normalized age-distribution curves for U-Pb dates on detrital zircons from Cretaceous sandstones in the Cretaceous foreland basin system of Utah–Colorado. The asterisks (*) denote data reported by Dickinson and Gehrels (2008).

The variations in carbonate $\delta^{13}C$ values shown by MCLs (Fig. 9) require that more than one source of dissolved inorganic carbon (DIC) was present in the shallow meteoric diagenetic systems in which these carbonates were stabilized. In these near-surface fresh groundwater systems, the two most likely sources of dissolved carbonate are an isotopically heavier end member introduced by the diffusion of atmospheric CO_2, and an isotopically lighter end member produced by root respiration of terrestrial flora and/or the microbial decay of the soil organic matter. Cerling and Quade (1993) reported that in all cases, the $\delta^{13}C$ value of soil CO_2 is heavier by 4.4 per mil or more than that of soil-respired CO_2.

At Price River, the standard deviations from the 40 mean $\delta^{13}C$ values ranged from 0.06 up to 1.8‰, with an average standard deviation of 0.36‰. These results indicate that differing proportionate contributions of isotopically heavy and light end-member DIC sources was not a major variable during the accumulation of these strata. Importantly, this also suggests that the $\delta^{13}C$ values of both atmospheric and soil-respired CO_2 were two major variables that changed concurrently during the deposition of the Cedar Mountain Formation, and that the "calcretes" in the Cedar Mountain Formation thus captured a record of changing paleoatmospheric $\delta^{13}C$ values.

Al-Suwaidi (2007) developed four overlapping chemostratigraphic $\delta^{13}C$ profiles of bulk organic matter isolated from carbonates in the Cedar Mountain Formation each of which overlap with part of our Price River section (Fig. 4), from about the 65 m to the 115 m stratigraphic levels. The results of the organic $\delta^{13}C$ analyses of Al-Suwaidi (2007) and the carbonate $\delta^{13}C$ analyses reported in this study are compared in Table 2 with typical pre-industrial $\delta^{13}C$ values for both C3 and C4 terrestrial floras reported by Koch (1998), and earlier results from the Cedar Mountain Formation reported by Ekart et al. (1999). The organic matter $\delta^{13}C$ values reported by Al-Suwaidi (2007) have a total range of over 11 per mil (−24.8 to −12.84‰ VPDB), while our carbonate $\delta^{13}C$ values have a total range of 4.8 per mil (−7.9 to −3.1‰ VPDB). Terrestrial plants utilizing the C4 photosynthetic pathway are commonly believed to have

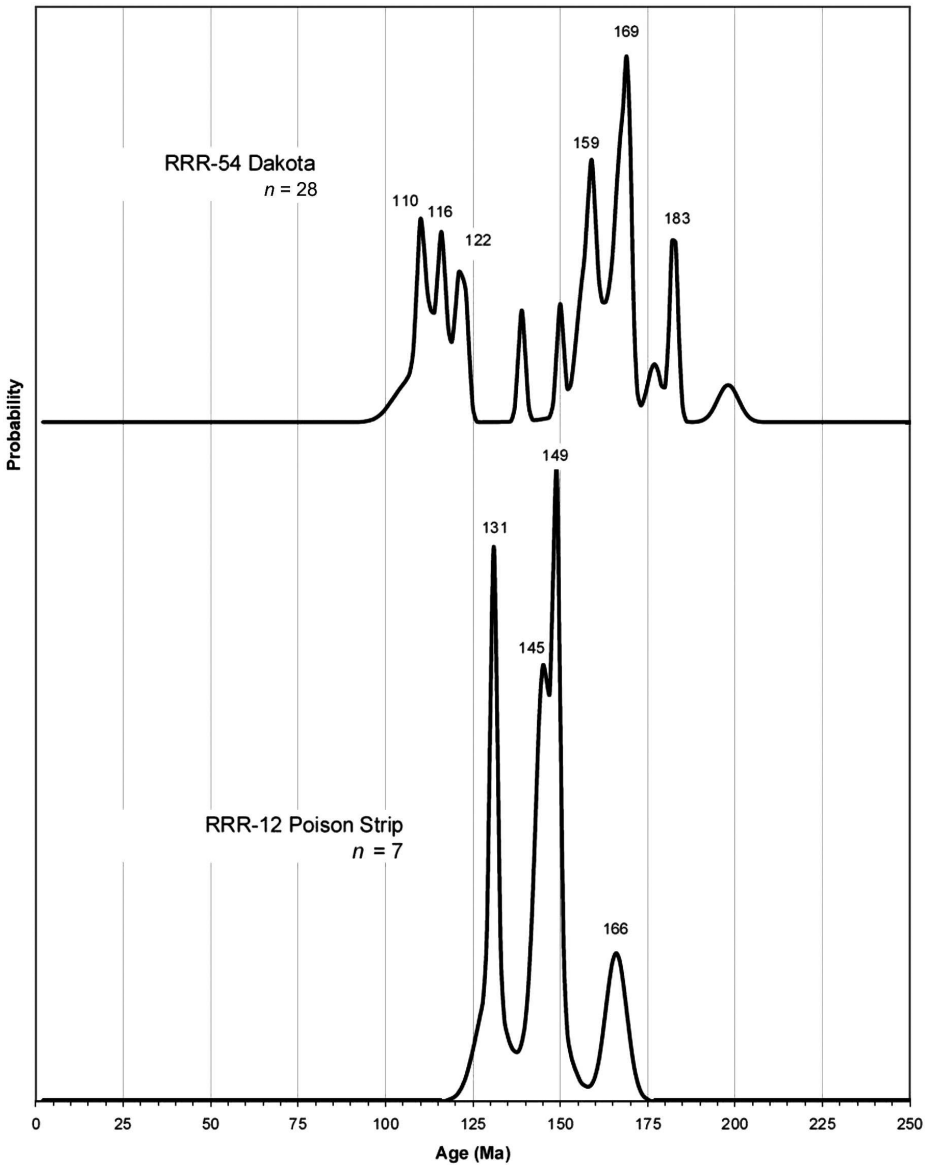

FIG. 12.—Normalized age-distribution curves for U-Pb dates on Mesozoic detrital zircons from Cretaceous sandstones at the Ruby Ranch Road section.

originated in the Neogene (Koch 1998), meaning that they theoretically were not part of the Cedar Mountain Formation paleoflora. The end-member $\delta^{13}C$ values and differences between carbonates and organic matter in the Cedar Mountain Formation at Price River (Table 2) do not readily conform to any simple model of terrestrial ecosystems dominated by either C3 or C4 paleofloras.

At present, there are large uncertainties in estimates of Early Cretaceous pCO_2 (Ekart et al. 1999; Royer et al. 2004), on variations in the carbon isotope compositions of the Early Cretaceous atmosphere (Ekart et al. 1999), and on the possible presence/influence of Cretaceous arid climate-adapted succulent plants using the CAM photosynthetic pathway in producing organic matter with $\delta^{13}C$ values higher than those of C3 floras (Koch 1998). Taken along with uncertainties on the extent of moisture stress on ^{13}C enrichments in Cretaceous C3 paleofloras, it is presently too early to speculate on paleo-pCO_2 changes during deposition of the Cedar Mountain Formation. Of

TABLE 2.—*Comparison of the carbon isotope values from modern and Early Cretaceous continental carbon-bearing materials.*

Sources	Soil Organic Matter	Soil Carbonate	Atmospheric CO_2
Preindustrial C3 continental environments (Koch 1998)	~ −26‰	~ −11‰	~ −6.5‰
Preindustrial C4 continental environments (Koch 1998)	~ −12‰	~ +3‰	~ −6.5‰
Maximum $\delta^{13}C$ at Price River Section (This study and Al-Suwaidi 2007)	−12.84‰	−3.1‰	?
Minimum $\delta^{13}C$ at Price River Section (This study and Al-Suwaidi 2007)	−24.8‰	−7.9‰	?
Aptian Cedar Mountain Formation, San Rafael Swell (Ekart et al. 1999)	−23.7‰	−5.7‰	−5.7‰

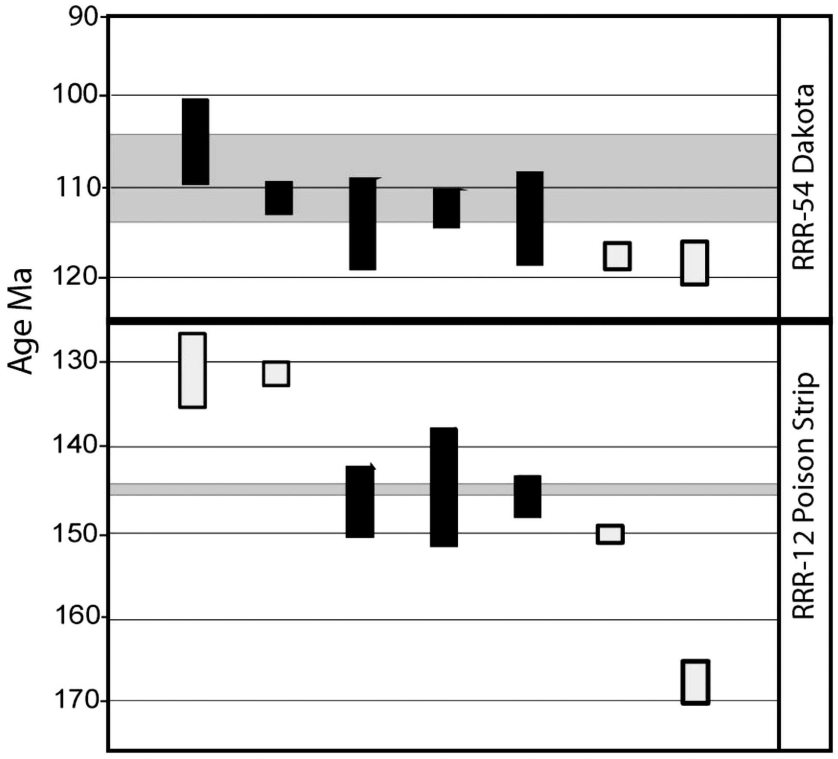

FIG. 13.—Maximum depositional ages (TuffZirc ages, Ludwig 2003) from the age spectra of U-Pb dates on detrital zircons in Cretaceous sandstones at the Ruby Ranch Road section. The maximum depositional age of the Poison Strip Sandstone (RRR-12) is 146 +0.49 −0.47 Ma (~ 75% confidence), and the maximum depositional age of the Dakota Sandstone is 112 +1.76 −6.73 Ma (~ 98% confidence). Confidence levels of 100% are based on all seven of the youngest grains overlapping in error (2σ). Confidence is 0% for two or fewer overlapping grains (Ludwig 2003).

special note, the chemostratigraphic profile from Ruby Ranch Road will eventually include a highly resolved coupling of organic matter and carbonate $\delta^{13}C$ data that might permit us to revisit these questions later in more detail.

Burial Diagenetic Products and Processes

Burial diagenetic spars in intraclastic packstones and tectonic vein calcites in rock samples PRC-23 and PRC-10 can be differentiated by $\delta^{18}O$ values that are lighter and more variable than those of the fine-grained matrix carbonates in these same rocks (Fig. 9). Their $\delta^{18}O$ values range from −11.3 up to −9.6‰ VPDB, and their $\delta^{13}C$ values approximate −6‰ VPDB, which also closely approximates the baseline $\delta^{13}C$ value for the chemostratigraphic profiles from Price River and Ruby Ranch Road. These components are collectively arrayed along horizontal linear trends in carbon–oxygen isotope space, trends that are conventionally interpreted to preserve records of burial diagenesis (Choquette and James 1990, p. 91–92). Lighter $\delta^{18}O$ values from these components, and the wider range of $\delta^{18}O$ variation found in them, suggests that they precipitated from a closed, rock-dominated diagenetic system at higher burial temperatures, with $\delta^{13}C$ values determined by the average carbonate rock $\delta^{13}C$ value from the Cedar Mountain Formation (cf. Choquette and James 1990; Algeo et al. 1992).

Chronostratigraphic Analysis

Maximum Depositional Age of the Poison Strip Sandstone.—A TuffZirc age of ~ 146 Ma (Fig. 13) for the Poison Strip Sandstone at Ruby Ranch Road postdates all tuff beds in the underlying Tithonian Brushy Basin Member of the Morrison Formation (Kowallis et al. 2008) and all detrital zircons in the same unit (Dickinson and Gehrels 2008). Additionally, the presence of two nearly identical Barremian grains (~ 131 Ma) shows that the Poison Strip Sandstone is younger than latest Tithonian, and supports most interpretations of Barremian–Aptian ages for the lower Cedar Mountain Formation fluvial system (Fig. 10; Currie 1998; Kirkland and Madsen 2007; Greenhalgh et al. 2006; Dickinson and Gehrels 2008).

Importantly, detrital zircon sample RRR-12 occurs a few meters *above* sample RRR-8, which produced a carbonate U-Pb date of 119.4 ± 2.6 Ma. The results of these two independent dating techniques are compatible, and show conclusively that the basal sampled strata at Ruby Ranch Road are early Aptian in age.

Maximum Depositional Age of the Dakota Sandstone.—A TuffZirc age of ~ 112–106 Ma (sample RRR-54) dates Dakota Formation deposition at Ruby Ranch Road to an early–mid-Albian maximum (Fig. 13), with a youngest grain ~ 105 Ma. Abundant Mesozoic grains (~ 30%) reflect culminations of Cretaceous arc and Jurassic back-arc magmatism in the Cordillera (Armstrong and Ward 1993), and perhaps direct fluvial transport from southwesterly Mesozoic plutons and the recycling of arc grains from intrabasinal tuffs. Finally, because Mesozoic grains are absent in Jurassic eolian sediments (Dickinson and Gehrels 2003), diverse distributions of arc-derived grains in sandstones from Ruby Ranch Road indicate provenance shifts between Barremian–Aptian and Albian–Cenomanian sandstones (Fig. 12).

The detrital-zircon population from sample RRR-54 demonstrates that the Ruby Ranch Member at Ruby Ranch Road spans upward through the middle to late Albian, and therefore the section should record early Aptian–early Albian global change events.

Radiometric Dates and Carbon Isotope Chemostratigraphy.—Radiometric dates from the Cedar Mountain Formation are shown in relation to Cretaceous chronostratigraphy and C-isotope stratigraphy from Leckie et al. (2002) in Figure 14. The most important constraint comes from the early Aptian 119.4 ± 2.6 Ma U-Pb date on carbonate from the position of sample RRR-8. The determination of maximum depositional ages (Gehrels et al. 2006) on detrital zircons (TuffZirc algorithm of Ludwig 2003) overestimates actual depositional ages. Nonetheless, the

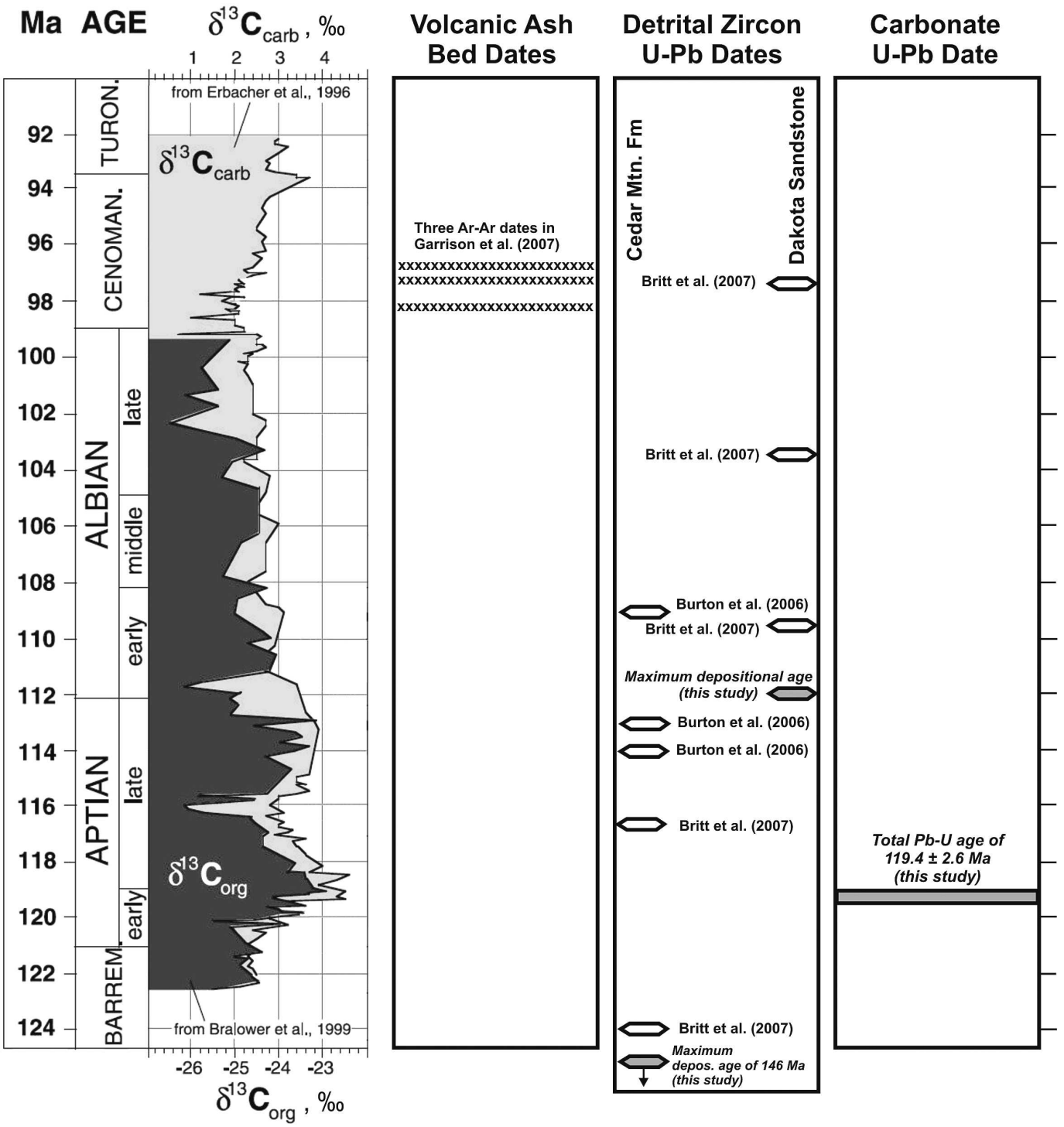

FIG. 14.—Compilation of radiometric dates from the Cretaceous Cedar Mountain Formation compared with the Aptian–Albian $\delta^{13}C$ chemostratigraphy from Leckie et al. (2002). The left panels are reproduced and modified from Leckie et al. (2002), and are used with the author's permission. Dates shown in black and white are from published sources, and the symbols with green fill are from the present study. In aggregate, the data show that the Cedar Mountain Formation spans through the Aptian Stage, and should be expected to overlap with the early and late Aptian positive $\delta^{13}C$ excursions.

maximum depositional ages derived from detrital zircons provide important geochronological constraints on stratigraphic sections. The maximum depositional ages of ~ 146 Ma (RRR-12, with grains as young as ~ 131 Ma) and ~ 112 Ma (RRR-54, with grains as young as ~ 105 Ma) further show that the sampled stratigraphic section at Ruby Ranch Road overlaps with long-ranging global positive carbon isotope excursions in the early Aptian and late Aptian–early Albian (Fig. 14). Three $^{40}Ar/^{39}Ar$ volcanic-ash-bed dates reported by Garrison et al. (2007) from the Mussentuchit Member span from 98.5 to 96.7 Ma and place that unit in the Cenomanian Stage.

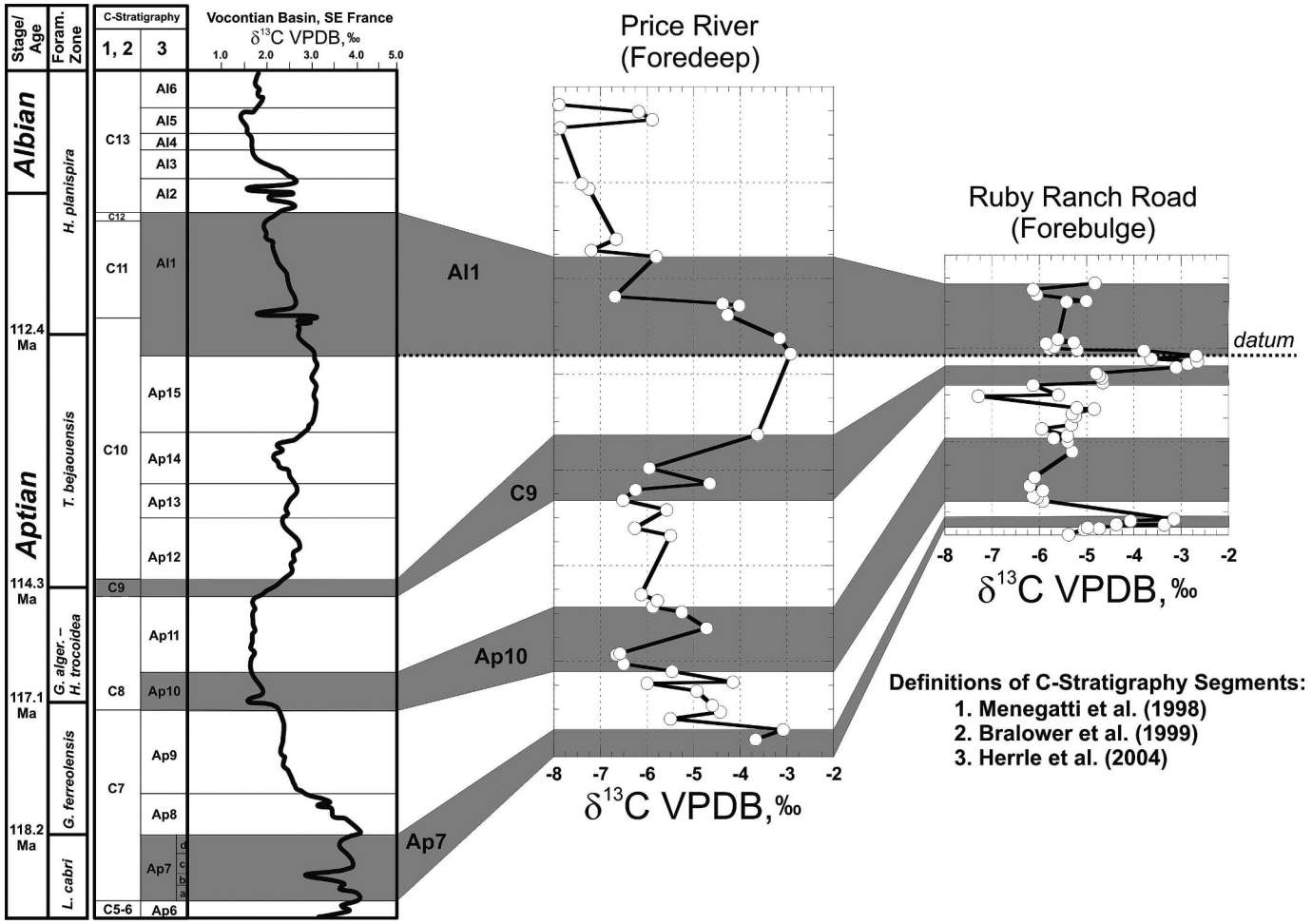

FIG. 15.—Correlation of high-resolution C-isotope stratigraphy from the Vocontian Basin of SE France (Herrle et al. 2004) with the C-isotope chemostratigraphy of the Cedar Mountain Formation at the Price River and Ruby Ranch Road sections. The curve from Herrle et al. (2004) is a ten-point moving average.

Carbon Isotope Correlations.—The Aptian–Albian carbon isotope stratigraphy of stratigraphic sections at Price River and Ruby Ranch Road are compared with a high-resolution record from SE France by Herrle et al. (2004) in Figure 15. Certain carbon isotope segments or features, but not all of them, are confidently correlated into the Cedar Mountain Formation.

The early Aptian Ap7 feature of Herrle et al. (2004) corresponds with a closely spaced double-peak positive carbon isotope excursion (CIE), and is recognized in the lowermost parts of both stratigraphic sections of the Cedar Mountain Formation by $\delta^{13}C$ values up to −3‰ VPDB (Fig. 15). This interval contains the carbonate bed at position RRR-8 that produced a U-Pb date of 119.4 ± 2.6 Ma, which closely matches to the double peak in $\delta^{13}C$ values from the global carbon isotope chronology (Fig. 14). The top of Ap7 carbon isotope feature of Herrle et al. (2004) closely corresponds with the boundary between the *L. cabri* and *G. ferreolensis* foraminiferal zones, dated at 118.2 Ma by Leckie et al. (2002). The Ap7 feature occurs in the lowermost sampled units of the Ruby Ranch Member at Price River, and probably extends downward into underlying unsampled coarse-grained units of the Buckhorn Conglomerate (Fig. 16), so its thickness there is not known. At Ruby Ranch Road, the Ap7 feature occurs through an interval of about 2 meters in thickness at the base of the Poison Strip Sandstone, from about the 2 to 4 meter stratigraphic levels (Fig. 16).

The late Aptian Ap10 feature of Herrle et al. (2004) includes a relatively abrupt negative CIE that is embedded within a long-ranging trend of decreasing $\delta^{13}C$ values spanning from the Ap8 to Ap11 features. It is easily recognized at Price River, and even though there are significant gaps in the sampling frequency at Ruby Ranch Road, it is recognized by the occurrence of an interval with $\delta^{13}C$ values lower than −6‰ VPDB (Fig. 15). The negative CIE at the Ap10 feature of Herrle et al. (2004) closely corresponds with the boundary between the *G. ferreolensis* and *G. algerianus* foraminiferal zones, dated at 117.1 Ma by Leckie et al. (2002). At Price River, the negative CIE of the Ap10 feature extends from about the 19 to 32 m stratigraphic levels, possibly even more due to covered section (Fig. 16). At Ruby Ranch Road, the negative CIE of the Ap10 feature extends from about the 7 to 21 m stratigraphic levels (Fig. 16).

The late Aptian C9 segment of Bralower et al. (1999) represents the abrupt rising limb of a major long-ranging positive CIE that appears above a long-ranging trend of decreasing $\delta^{13}C$ values of the Ap8 to Ap11 features of Herrle et al. (2004). The C9 segment is easily recognized in both sections of the Cedar Mountain Formation by an abrupt upward increase in $\delta^{13}C$ values from below −6‰ to above −4‰ VPDB (Fig. 15). The C9 segment of Bralower et al. (1999) corresponds with the base of the *T. bejaouensis* foraminiferal zone, dated at 114.3 Ma by Leckie et al. (2002). At Price River, the C9 segment of Bralower et al. (1999) extends from about the 48 to 66 m stratigraphic levels, while at Ruby Ranch

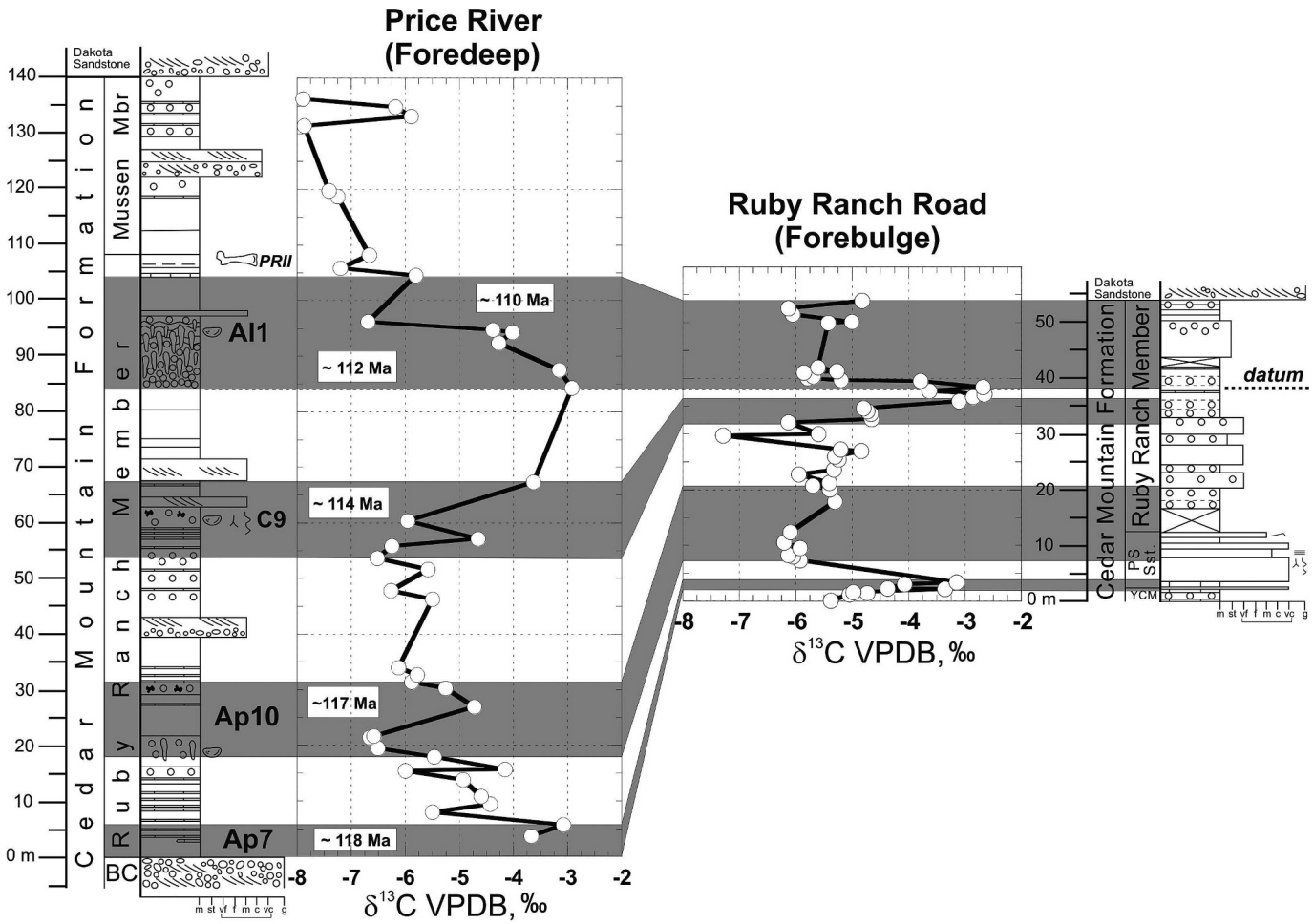

FIG. 16.—Correlation of high-resolution Aptian–Albian C-isotope stratigraphy and lithostratigraphy between the Price River and Ruby Ranch Road sections. Highly generalized ages bounding the upper limits of the Ap7 (~ 118 Ma), Ap10 (~ 117 Ma), and C9 (~ 114 Ma) features of Herrle et al. (2004) are shown, along with the lower (~ 112 Ma) and upper (~ 110 Ma) limits of the Al1 feature of Herrle et al. (2004).

Road, the C9 segment extends from about the 32 to 37 m stratigraphic levels (Fig. 16).

The latest Aptian Al1 feature of Herrle et al. (2004) lies at a break point separating an underlying long-term trend of rising $\delta^{13}C$ values from an overlying long-term trend of falling $\delta^{13}C$ values, including the falling limb of the major latest Aptian positive CIE (C11 segment of Bralower et al. 1999). It also includes short-term negative and positive CIEs that also define its upper limit. The base of the Al1 feature is confidently recognized in both sections of the Cedar Mountain Formation by peak $\delta^{13}C$ values higher than −3‰ VPDB, and we utilize it as a stratigraphic datum (Figs. 15, 16). Herrle et al. (2004) also proposed that the specific horizon of this break point be considered as an alternative global definition of the Aptian–Albian stage boundary, in view of the long-standing problems of endemism and diachronous appearances that complicate applications of the standard biostratigraphic indicators. The base of the Al1 feature (Herrle et al. 2004) occurs below the boundary between the *T. bejaouensis* and *H. planispira* foraminiferal zones, dated at 112.4 Ma by Leckie et al. (2002). Erbacher and Thurow (1997) illustrated $\delta^{13}C$ chemostratigraphic features from the Umbria–Marche Basin of central Italy that closely match with the top the Al1 feature of Herrle et al. (2004), and which culminate with the deposition of the early Albian OAE 1b black shale. Erbacher and Thurow (1997) showed this position as corresponding with the base of the *T. primula* foraminiferal zone, dated at 109.5 Ma by Leckie et al. (2002). These observations suggest an early Albian age for the top of the Al1 segment of ~ 109.5 Ma, and possibly as old as 111 Ma (Mark Leckie, personal communication 2009).

At Price River, the Al1 feature of Herrle et al. (2004) extends from about the 84 to 104 m stratigraphic levels, while at Ruby Ranch Road, the Al1 feature extends from about the 38 to 54 m stratigraphic levels up to the erosional base of the Dakota Sandstone (Fig. 16). At Price River, the Al1 feature terminates just below the position of the Price River II dinosaur quarry (Fig. 16; Kirkland and Madsen 2007), thus dating this important local succession of bone beds as early Albian with an age of at least 109.5 Ma.

The structure of the Price River and Ruby Ranch Road chemostratigraphic profiles shows a generally proportionate thinning of individual chemostratigraphic features from the foredeep on to the forebulge, suggesting that there were consistently lower rates of sediment accumulation on the forebulge during the Aptian–Albian stages. The most abrupt thinning of strata on the forebulge appears to be during the intervals of the Ap8–Ap9 and Ap12–Ap15 features (Fig. 15).

Paleoclimatic Implications.—Aptian–Albian positive CIEs in the Cedar Mountain Formation are associated with coeval shifts toward higher micritic calcite $\delta^{18}O$ values (Ludvigson et al. 2003), with magnitudes in the 3 to 4 per mil range. Moreover, these authors suggested that these

phenomena recorded local aridification events in the terrestrial environments of the North American foreland-basin system. Critical evaluation of these paleoclimatic data must necessarily follow the formally published chronostratigraphic correlation of hosting terrestrial strata.

Aptian–Albian chemostratigraphic correlations in the Cedar Mountain Formation serve as the temporal framework for interpreting the coordinated $\delta^{13}C$ and $\delta^{18}O$ data from the Cedar Mountain Formation and the diagenetic and paleohydrologic processes that they record. The CIEs in the Cedar Mountain Formation provide an empirical foundation for directly interpreting the terrestrial paleoclimatic consequences of the major carbon-cycle perturbations of the mid-Cretaceous (Dumitrescu et al. 2006; Ando et al. 2008). The integration of paleopedologic and stable-isotope diagenetic and paleohydrologic investigations of the terrestrial strata of the Cedar Mountain Formation and other coeval terrestrial units promises to open a new avenue for better understanding the global paleoclimate dynamics of the Cretaceous greenhouse world.

CONCLUSIONS

- U-Pb dating of terrestrial carbonates and detrital zircons bracket the elapsed geologic time represented by Cedar Mountain Formation strata at Ruby Ranch Road. These dates constrain a lower, older age from the Poison Strip Sandstone (119.4 ± 2.6 Ma) and an upper, younger age from the Ruby Ranch Member (~ 106 Ma) of the Cedar Mountain Formation. These absolute ages permit refined Aptian–Albian chronostratigraphic correlations in the Cedar Mountain Formation by carbon isotope chemostratigraphy.
- Carbon isotope excursions (CIEs) in chemostratigraphic profiles from the continental Cedar Mountain Formation correlate with the Aptian–Albian Ap7, Ap10, C9, and Al1 features of the global carbon isotope stratigraphy. Therefore, we surmise that widespread application of carbon isotope chemostratigraphy is practicable for the chronostratigraphic correlation of Aptian–Albian continental strata.
- Nodular carbonates (“calcretes”) of the Cedar Mountain Formation are of palustrine origins and record authigenic cementation in early meteoric phreatic and vadose environments. Meteoric calcite lines (MCLs) with $\delta^{18}O$ values ranging between −8.1 to −7.5‰ VPDB indicate calcite crystallization in shallow groundwaters with $\delta^{18}O$ values of ~ −6‰ VSMOW—the zonal mean for Cretaceous paleoprecipitation at 34° N paleolatitude.
- The ranges of $\delta^{13}C$ values for MCLs in the Cedar Mountain Formation show stratigraphic trends, recording concurrent trends in the $\delta^{13}C$ values of atmospheric CO_2, soil organic matter, and soil-respired CO_2. Concurrent shifts in the $\delta^{13}C$ values of these terrestrial carbon pools generated the overall structure of the chemostratigraphic profiles.
- The CIEs in the Cedar Mountain Formation identify narrow stratigraphic intervals recording the terrestrial paleoclimatic impacts of ancient global change events. The Ap7 and C9-Al1 positive CIEs in the Cedar Mountain Formation coincide with short-term shifts toward higher $\delta^{18}O$ values, which provide direct evidence for aridification events.
- Our carbon isotope stratigraphy demonstrates that Cedar Mountain Formation strata correlate, but also thin, from the foredeep to the forebulge of the North American foreland basin. There is no conclusive evidence for local uplift and erosional beveling of strata in the foreland basin during Cedar Mountain Formation times.
- Palustrine carbonates in the Cedar Mountain Formation, and probably in other continental strata, preserve time-averaged records of early diagenesis that are integrated at time scales of 10^4 to 10^5 years, and therefore they can be used to resolve terrestrial records of Cretaceous and other ancient CIEs.

ACKNOWLEDGMENTS

Our work on the Cedar Mountain Formation has been supported by US National Science Foundation grants EAR-9628128 and EAR-0325072, and the National Science Foundation Research Experience for Undergraduates (REU) Program hosted by the University of Iowa Center for Global & Regional Environmental Research through grant EEC-9912191. We thank REU students Liz Smith and Andy Sorensen for field and laboratory assistance in 2001–2002. While Ludvigson and González were located at the University of Iowa, their work on the Cedar Mountain Formation was supported by many associates including Scott Carpenter, Kay Saville, Vicki Grassian, Greg Carmichael, David Ufnar, Brian Witzke, Bob Brenner, and Jeremy Davis. At the University of Kansas, our efforts have been aided by Laura Murphy, Jon J. Smith, Wayne Dickerson, Arlo McKee, Greg Cane, Aisha Al-Suwaidi, Marina Suarez, Celina Suarez, and Emily Tremain. The work of Hunt was aided by Tim Lawton, George Gehrels, and Victor Valencia. Pat Acker of the Kansas Geological Survey assisted in preparation of figures. We thank JSR editors Paul McCarthy, Peter Mozley, and John Southard, and reviewers Greg Price and Mark Leckie, for constructive criticism that substantially improved our presentation.

REFERENCES

Algeo, T.J., Wilkinson, B.H., and Lohmann, K.C., 1992, Meteoric-burial diagenesis of Middle Pennsylvanian limestones in the Orogrande Basin, New Mexico: water/rock interactions and basin geothermics: Journal of Sedimentary Petrology, v. 62, p. 652–670.

Al-Suwaidi, A.H., 2007, A ped’s story: weathering out climatic change during the mid-Cretaceous [unpublished M.S. thesis]: University of Kansas, Lawrence, Kansas, 134 p.

Amiot, R., Lecuyer, C., Escarguel, G., Billon-Bruyat, J.P., Buffetaut, E., Langlois, C., Martin, S., Martineau, F., and Mazin, J.M., 2007, Oxygen isotope fractionation between crocodilian phosphate and water: Palaeogeogeography, Palaeoclimatology, Palaeoecology, v. 243, p. 412–420.

Ando, A., Kakegawa, T., Takashima, R., and Saito, T., 2002, New perspective on Aptian carbon isotope stratigraphy: data from $\delta^{13}C$ records of terrestrial organic matter: Geology, v. 30, p. 227–230.

Ando, A., Kaiho, K., Kawahata, H., and Kakegawa, T., 2008, Timing and magnitude of early Aptian extreme warming: unraveling primary $\delta^{18}O$ variation in indurated pelagic carbonates at Deep Sea Drilling Project Site 463, central Pacific Ocean: Palaeogeography, Palaeoclimatology, Palaeoecology, v. 260, p. 463–476.

Armstrong, R.L., and Ward, P.L., 1993, Late Triassic to earliest Eocene magmatism in the North American Cordillera: implications for the Western Interior Basin, *in* Caldwell, W.G.E., and Kauffman, E.G., eds., Evolution of the Western Interior Basin, Geological Association of Canada, Special Paper 39, p. 49–72.

Bains, S., Norris, R.D., Corfield, R.M., Bowen, G.J., Gingerich, P.D., and Koch, P.L., 2003, Marine–terrestrial linkages at the Paleocene–Eocene boundary, *in* Wing, S.L., Gingerich, P.D., Schmitz, B., and Thomas, E., eds., Causes and Consequences of Globally Warm Climates in the Early Paleogene, Geological Society of America, Special Paper 369, p. 1–9.

Barrick, R.E., Fisher, A.L., and Showers, W.J., 1999, Oxygen isotopes from turtle bone: applications for terrestrial paleoclimates: Palaios, v. 14, p. 186–191.

Bodily, N.M., 1969, An armored dinosaur from the Lower Cretaceous of Utah: Brigham Young University, Geology Studies, v. 16, p. 35–60.

Boggs, S, Jr, and Krinsley, D., 2006. Application of Cathodoluminescence Imaging to the Study of Sedimentary Rocks: Cambridge, UK, Cambridge University Press, 165 p.

Bralower, T.J., Cobabe, E., Clement, B., Sliter, W.V., Osburn, C.L., and Longoria, J., 1999, The record of global change in mid-Cretaceous (Barremian–Albian) sections from the Sierra Madre, northeastern Mexico: Journal of Foraminiferal Research, v. 29, p. 418–437.

Britt, B.B., and Stadtman, K.L., 1997, Dalton Wells quarry, *in* Currie, P.J., and Padian, K., eds., Encyclopedia of Dinosaurs: San Diego, Academic Press, p. 165–166.

Britt, B.B., Stadtman, K.L., and Scheetz, R.D., 1997, The Early Cretaceous Dalton Wells dinosaur fauna and the earliest North American titanosaurid sauropod [abstract]: Journal of Vertebrate Paleontology, v. 16, Supplement to No. 3, 24A p.

Britt, B.B., Burton, D., Greenhalgh, B.W., Kowallis, B.J., Christiansen, E., and Chure, D.J., 2007, Detrital zircon ages for the basal Cedar Mountain Formation (Early Cretaceous) near Moab, and Dinosaur National Monument, Utah (abstract): Geological Society of America, Abstracts with Programs, v. 39, no. 5, 16 p.

Budd, D.A., Pack, S.M., and Fogel, M.L., 2002, The destruction of paleoclimatic isotopic signals in Pleistocene carbonate soil nodules of Western Australia: Palaeogeography, Palaeoclimatology, Palaeoecology, v. 188, p. 249–273.

Carpenter, K., Kirkland, J.I., Burge, D., and Bird, J., 1999, Ankylosaurs (Dinosauria: Ornithischia) of the Cedar Mountain Formation, Utah, and their stratigraphic distribution, *in* Gillette, D., ed., Vertebrate Paleontology in Utah, Utah Geological Survey, Miscellaneous Publication 99-1, p. 243–251.

Cerling, T.E., and Quade, J., 1993, Stable carbon and oxygen isotopes in soil carbonates, *in* Swart, P.K., Lohmann, K.C., McKenzie, J., and Savin, S., eds., Climate Change in Continental Isotopic Records, American Geophysical Union, Geophysical Monograph 78, p. 217–231.

Choquette, P.W., and James, N.P., 1990, Limestones—The burial diagenetic environment, *in* McIlreath, I.A., and Morrow, D.W., eds., Diagenesis, Geoscience Canada Reprint Series 4, Geological Association of Canada, Ottawa, Ontario, p. 75–112.

Cifelli, R.L., and de Muizon, C., 1997, Dentition and jaw of *Kokopellia juddi*, a primitive marsupial or near-marsupial from the medial Cretaceous of Utah: Journal of Mammalian Evolution, v. 4, p. 241–258.

Cifelli, R.L., Kirkland, J.I., Weil, A., Deinos, A.R., and Kowallis, B.J., 1997, High-precision $^{40}Ar/^{39}Ar$ geochronology and the advent of North America's Late Cretaceous terrestrial fauna: National Academy of Science, USA, Proceedings, v. 94, p. 11163–11167.

Cifelli, R.L., Nydam, R.L., Gardner, J.D., Weil, A., Eaton, J.G., Kirkland, J.I., and Madsen, S.K., 1999, Medial Cretaceous vertebrates from the Cedar Mountain Formation, Emery County, the Mussentuchit local fauna, *in* Gillette, D., ed., Vertebrate Paleontology in Utah, Utah Geological Survey, Miscellaneous Publication 99-1, p. 219–242.

Cobban, W.A., and Kennedy, W.J., 1989, The ammonite *Metengonoceras* Hyatt, 1903 from the Mowry Shale (Cretaceous) of Montana and Wyoming: U.S. Geological Survey, Professional Paper 1787L, 11 p.

Cojan, I., Moreau, M.-G., and Stott, L.E., 2000, Stable carbon isotope stratigraphy of the Paleogene pedogenic series of southern France as a basis for continental–marine correlation: Geology, v. 28, p. 259–262.

Cole, J.M., Nienstedt, J., Spataro, G., Rasbury, E.T., Lanzirotti, A., Celestian, A.J., Nilsson, M., and Hanson, G.N., 2003, Phosphor imaging as a tool for in situ mapping of ppm levels of uranium and thorium in rocks and minerals: Chemical Geology, v. 193, p. 127–136.

Cole, J.M., Rasbury, E.T., Hanson, G.N., Montañez, I.P., and Pedone, V.A., 2005, Using U-Pb ages of Miocene tufa for a correlation in a terrestrial succession, Barstow Formation, California: Geological Society of America, Bulletin, v. 117, p. 276–287.

Currie, B.S., 1998, Upper Jurassic–Lower Cretaceous Morrison and Cedar Mountain Formations, NE Utah–NW Colorado: relationships between nonmarine deposition and early Cordilleran foreland basin development: Journal of Sedimentary Research, v. 68, p. 632–652.

Currie, B.S., 2002, Structural configuration of the Early Cretaceous cordilleran foreland-basin system and Sevier Thrust Belt, Utah and Colorado: Journal of Geology, v. 110, p. 697–718.

Dickinson, W.R., and Gehrels, G.E., 2003, U-Pb ages of detrital zircons from Permian and Jurassic eolian sandstones of the Colorado Plateau, USA: paleogeographic implications: Sedimentary Geology, v. 163, p. 29–36.

Dickinson, W.R., and Gehrels, G.E., 2008, Sediment delivery to the Cordilleran foreland basin: insights from U-Pb ages of detrital zircons in Upper Jurassic and Cretaceous strata of the Colorado Plateau: American Journal of Science, v. 308, p. 1041–1082.

Dumitrescu, M., Brassell, S.C., Schouten, S., Hopmans, E.C., and Sinnighe Damsté, J.S., 2006, Instability in tropical Pacific sea-surface temperatures during the early Aptian: Geology, v. 34, no. 10, p. 833–836, doi: 10.1130/G22882.1.

Eberth, D.A., Britt, B.B., Scheetz, R., Stadtman, K.L., and Brinkman, D.B., 2006, Dalton Wells—geology and significance of debris-flow-hosted dinosaur bonebeds in the Cedar Mountain Formation (Lower Cretaceous) of eastern Utah, USA: Paleogeography, Paleoclimatology, Paleoecology, v. 236, p. 217–245.

Ekart, D.D., Cerling, T.E., Montañez, I.P., and Tabor, N.J., 1999, A 400 million year carbon isotope record of pedogenic carbonate: implications for paleoatmospheric carbon dioxide: American Journal of Science, v. 299, p. 805–827.

Elliot, W.S, Jr, Suttner, L.J., and Pratt, L.M., 2007, Tectonically induced climate and its control on the distribution of depositional systems in a continental foreland basin, Cloverly and Lakota formations (Lower Cretaceous) of Wyoming, U.S.A.: Sedimentary Geology, v. 202, p. 730–753.

Erbacher, J., and Thurow, J., 1997, Influence of oceanic anoxic events on the evolution of mid-Cretaceous radiolaria in the North Atlantic and western Tethys: Marine Micropaleontology, v. 30, p. 139–158.

Erbacher, J., Thurow, J., and Littke, R., 1996, Evolution patterns of radiolaria and organic matter variations: a new approach to identify sea-level changes in mid-Cretaceous pelagic environments: Geology, v. 24, p. 499–502.

Galton, P.M., and Jensen, J.A., 1979, Remains of ornithopod dinosaurs from the Lower Cretaceous of North America: Brigham Young University, Geology Studies, v. 25, p. 1–10.

Garrison, J.R, Jr, Brinkman, D., Nichols, D.J., Layer, P., Burge, D., and Thayn, D., 2007, A multidisciplinary study of the Lower Cretaceous Cedar Mountain Formation, Mussentuchit Wash, Utah: a determination of the paleoenvironment and paleoecology of the *Eolambia caroljonesa* dinosaur quarry: Cretaceous Research, v. 28, p. 461–494.

Gehrels, G., Valencia, V., and Pullen, A., 2006, Detrital zircon geochronology by laser ablation multicollector ICPMS at the Arizona LaserChron Center, *in* Olszewski, T., ed., Geochronology: Emerging Opportunities, Paleontology Society Papers, Volume 12, p. 67–76.

Goudie, A.L., Viles, H., Allison, R., Day, M., Livingstone, I., and Bull, P., 1990, The geomorphology of the Napier Range, Western Australia: Institute of British Geographers, Transactions, New Series, v. 15, p. 308–322.

Greenhalgh, B.W., and Britt, B.B., 2007, Stratigraphy and sedimentology of the Morrison–Cedar Mountain Formation boundary, east-central Utah, *in* Willis, G.C., Hylland, M.D., Clark, D.L., and Chidsey, T.C, Jr, eds., Central Utah—Diverse Geology of a Dynamic Landscape, Utah Geological Association, Publication 36, p. 81–100.

Greenhalgh, B.W., Britt, B.B., and Kowallis, B.J., 2006, New U-Pb age control for the lower Cedar Mountain Formation and an evaluation of the Morrison Formation/Cedar Mountain Formation boundary, Utah (abstract): Geological Society of America, Abstracts with Programs, v. 38, no. 6, 7 p.

Gröcke, D.R., 2002, The carbon isotope composition of ancient CO_2 based on higher-plant organic matter: Royal Society of London, Philosophical Transactions, v. 360, p. 633–658.

Gröcke, D.R., Hesselbo, S.P., and Jenkyns, H.C., 1999, Carbon-isotope composition of Lower Cretaceous fossil wood: ocean–atmosphere chemistry and relation to sea-level change: Geology, v. 27, p. 155–158.

Gröcke, D.R., Ludvigson, G.A., Witzke, B.J., Robinson, S.R., Joeckel, R.M., Ufnar, D.F., and Ravn, R.L., 2006, Recognizing the Albian–Cenomanian (OAE1d) sequence boundary using plant carbon isotopes: Dakota Formation, Western Interior Basin, USA: Geology, v. 34, p. 193–196.

Hasegawa, T., 1997, Cenomanian–Turonian carbon isotope events recorded in terrestrial organic matter from northern Japan: Palaeogeography, Palaeoclimatology, Palaeoecology, v. 130, p. 251–273.

Heimhofer, U., Hochuli, P.A., Burla, S., Andersen, N., and Weissert, H., 2003, Terrestrial carbon-isotope records from coastal deposits (Algarve, Portugal): a tool for chemostratigraphic correlation on an intrabasinal and global scale: Terra Nova, v. 15, p. 8–13.

Herrle, J.O., Kößler, P., Friedrich, O., Erleneuser, H., and Hemleben, C., 2004, High-resolution carbon isotope records of the Aptian to Lower Albian from SE France and the Mazagan Plateau (DSDP Site 545): a stratigraphic tool for paleoceanographic and paleobiologic reconstruction: Earth and Planetary Science Letters, v. 218, p. 149–161.

Hofmann, P., Stüsser, I., Wagner, T., Schouten, S., and Sinninghe Damsté, J.S., 2008, Climate–ocean coupling off north-west Africa during the lower Albian: the Oceanic Anoxic Event 1b: Palaeogeography, Palaeoclimatology, Palaeoecology, v. 262, p. 157–165.

Hunt, G.J., and Lawton, T.F., 2008, Detrital zircon geochronology of Lower Cretaceous conglomerates, San Rafael Swell and Wasatch Plateau, central Utah, implications for conglomerate correlation and detrital sources [abstract]: Geological Society of America, Abstracts with Programs, v. 40, no. 1, 56 p.

Jacobs, L.L., Ferguson, K., Polcyn, M.J., and Rennison, C., 2005, Cretaceous $\delta^{13}C$ stratigraphy and the age of dolichosaurs and early mosasaurs: Geologie en Mijnbouw, v. 84, p. 257–268.

Jahren, A.H., Arens, N.C., Sarmiento, G., Guerrero, J., and Amundson, R., 2001, Terrestrial record of methane hydrate dissociation in the Early Cretaceous: Geology, v. 29, p. 159–162.

James, N.P., and Choquette, P.W., 1990, Limestones–The Meteoric Environment, *in* McIlreath, I.A., and Morrow, D.W., eds., Diagenesis, Geoscience Canada Reprint Series 4, Geological Association of Canada, Ottawa, Ontario, p. 35–74.

Jennings, J.N., and Sweeting, M.M., 1961, Caliche pseudo-anticlines in the Fitzroy Basin, Western Australia: American Journal of Science, v. 259, p. 635–639.

Kirkland, J.I., 2005, Dinosaurs from the Lower Cretaceous Cedar Mountain Formation: Moab, Utah: Dan O'Laurie Museum, Canyon Legacy, v. 55, p. 28–36.

Kirkland, J.I., and Madsen, S.K., 2007, The Lower Cretaceous Cedar Mountain Formation, eastern Utah: the view up an always interesting learning curve: Utah Geological Association, Publication 35, p. 1–108, (Field trip guide for 2007 Geological Society of America, Rocky Mountain Section, Annual Meeting, St. George, Utah, May 4–6, 2007.)

Kirkland, J.I., Burge, D., and Gaston, R., 1993, A large dromaeosaurid (Theropoda) from the Lower Cretaceous of Eastern Utah: Hunteria, v. 2, 16 p.

Kirkland, J.I., Britt, B., Burge, D., Carpenter, K., Cifelli, R., DeCourten, F., Eaton, J., Hasiotis, S., and Lawton, T., 1997, Lower to Middle Cretaceous dinosaur faunas of the Central Colorado Plateau: a key to understanding 35 million years of tectonics, sedimentology, evolution, and biogeography: Brigham Young University, Geology Studies, v. 42, p. 69–103.

Kirkland, J.I., Lucas, S.G., and Estep, J.W., 1998, Cretaceous dinosaurs of the Colorado Plateau, *in* Lucas, S.G., Kirkland, J.I., and Estep, J.W., eds., Lower to Middle Cretaceous Non-Marine Cretaceous Faunas, New Mexico Museum of Natural History and Science, Bulletin 14, p. 67–89.

Kirkland, J.I., Cifelli, R., Britt, B.B., Burge, D.L., DeCourten, F., Eaton, J., and Parrish, J.M., 1999, Distribution of vertebrate faunas in the Cedar Mountain Formation, east-central Utah, *in* Gillette, D., ed., Vertebrate Paleontology in Utah, Utah Geological Survey, Miscellaneous Publication 99-1, p. 201–217.

Kirkland, J.I., Zanno, L.E., Sampson, S.D., Clark, J.M., and DeBlieux, D.D., 2005, A primitive therizinosauroid dinosaur from the Early Cretaceous of Utah: Nature, v. 435, p. 84–87.

Koch, P.L., 1998, Isotopic reconstruction of past continental environments: Annual Reviews of Earth and Planetary Sciences, v. 26, p. 573–613.

Kowallis, B.J., Britt, B.B., Greenhalgh, B.W., and Sprinkel, D.A., 2007, New U-Pb zircon ages from an ash bed in the Brushy Basin Member of the Morrison Formation near Hanksville, Utah, *in* Willis, G.C., Hylland, M.D., Clark, D.L., and Chidsey, T.C, Jr, eds., Central Utah—Diverse Geology of a Dynamic Landscape, Utah Geological Association, Publication 36, p. 75–80.

Lawton, T.F., and Willis, G.C., 1987, The geology of Salina Canyon, Utah: Centennial Field Guide, Rocky Mountain Section of the Geological Society of America, v. 2, p. 265–268.

Leckie, R.M., Bralower, T.J., and Cashman, R., 2002, Oceanic anoxic events and plankton evolution: Biotic response to tectonic forcing during the mid-Cretaceous: Paleoceanography, v. 17, no. 3, 10.1029/2001PA000623.

Lohmann, K.C., 1988, Geochemical patterns of meteoric diagenetic systems and their application to studies of paleokarst, *in* James, N.P., and Choquette, P.W., eds., Paleokarst: New York, Springer, p. 58–80.

Ludvigson, G.A., Jacobson, S.R., Witzke, B.J., and Gonzalez, L.A., 1996, Carbonate component chemostratigraphy and depositional history of the Ordovician Decorah Formation, Upper Mississippi Valley, *in* Witzke, B.J., Ludvigson, G.A., and Day, J., eds., Paleozoic Sequence Stratigraphy: Views from the North American Craton, Geological Society of America, Special Paper 306, p. 67–86.

Ludvigson, G.A., González, L.A., Kirkland, J.I., Joeckel, R.M., Carpenter, S.J., Madsen, S.K., and Maxson, J.A., 2003, Terrestrial carbonate records of the carbon isotope excursions associated with mid-Cretaceous (Aptian–Albian) oceanic anoxic events [abstract]: Geological Society of America, Abstracts with Programs, v. 35, no. 6, 289 p.

Ludvigson, G.A., Witzke, B.J., González, L.A., Carpenter, S.J., Schneider, C.L., and Hasiuk, F., 2004, Late Ordovician (Turonian–Chatfieldian) carbon isotope excursions and their stratigraphic and paleoceanographic significance: Palaeogeography, Palaeoclimatology, Palaeoecology, v. 210, p. 187–214.

Ludwig, K.R., 2003, User's Manual for Isoplot 3.00: A Geochronological Toolkit for Microsoft Excel: Berkeley Geochronology Center, Special Publication 4, Berkeley, California, 70 p.

Menegatti, A.P., Weissert, H., Brown, R.S., Tyson, R.V., Farrimond, P., Strasser, A., and Caron, M., 1998, High-resolution $\delta^{13}C$ stratigraphy through the early Aptian "Livello Selli" of the Alpine Tethys: Paleoceanography, v. 13, p. 530–545.

Nichols, D.J., and Sweet, A.R., 1993, Biostratigraphy of Upper Cretaceous nonmarine palynofloras in a north–south transect of the Western Interior Basin, *in* Caldwell, W.G.E., and Kauffman, E.G., eds., Evolution of the Western Interior Basin, Geological Association of Canada, Special Paper 39, p. 539–584.

Platt, N.H., and Wright, V.P., 1992, Palustrine carbonates and the Florida Everglades: Towards an exposure index for the fresh-water environment?: Journal of Sedimentary Petrology, v. 62, p. 1058–1071.

Royer, D.L., Berner, R.A., Montañez, I.P., Tabor, N.J., and Beerling, D.J., 2004, CO_2 as a primary driver of Phanerozoic climate: GSA Today, v. 14, p. 4–10.

Shapiro, R.S., Fricke, H.C., and Fox, K., 2009, Dinosaur-bearing oncoids from ephemeral lakes of the Lower Cretaceous Cedar Mountain Formation, Utah: Palaios, v. 24, p. 51–58.

Sprinkel, D.A., Weiss, M.P., Fleming, R.W., and Waanders, G.L., 1999, Redefining the Lower Cretaceous stratigraphy within the Central Utah Foreland Basin: Utah Geological Survey, Special Study 97, 21 p.

Stikes, W.M., 2006, Fluvial facies and architecture of the Poison Strip Sandstone, Lower Cretaceous Cedar Mountain Formation, Grand County, Utah: Utah Geological Survey, Miscellaneous Publication 06-2, 84 p, CD-ROM.

Stoops, G., 2003, Guidelines for Analysis and Description of Soil and Regolith Thin Sections: Soil Science Society of America, Madison, Wisconsin, USA, 184 p.

Suarez, C.A., 2010, Geochemical approaches to the study of life and death of dinosaurs from the Early Cretaceous Cedar Mountain Formation, Utah [Ph.D. Dissertation]: University of Kansas, Lawrence, Kansas, 205 p.

Suarez, M.B., González, L.A., Ludvigson, G.A., Vega, F.J., and Alvarado-Ortega, J., 2009, Isotopic composition of low-latitude paleoprecipitation during the Early Cretaceous: Geological Society of America, Bulletin, v. 121, p. 1584–1595.

Tidwell, V.C., Carpenter, K., and Brooks, W., 1999, New sauropod from the Lower Cretaceous of Utah, USA: Oryctos, v. 2, p. 21–37.

Tschudy, R.H., Tschudy, B.D., and Craig, L.C., 1984, Palynological evaluation of Cedar Mountain and Burro Canyon formations, Colorado Plateau: U.S. Geological Survey, Professional Paper 1281, 21 p.

Wagner, T., Herrle, J.O., Sinnighe Damsté, J.S., Schouten, S., Stüsser, I., and Hofmann, P., 2008, Rapid warming and salinity changes of Cretaceous surface waters in the subtropical North Atlantic: Geology, v. 36, p. 203–206.

Watts, N.L., 1977, Pseudo-anticlines and other structures in some calcretes of Botswana and South Africa: Earth Surface Processes, v. 2, p. 63–74.

Wright, V.P., 2007, Calcrete, *in* Nash, D.J., and McLaren, S.J., eds., Geochemical Sediments and Landscapes: Oxford, U.K., Blackwell, p. 10–45.

Received 13 August 2009; accepted 5 July 2010.